Resum

El nivell de sedació en pacients sotmesos a procediments mèdics evoluciona contínuament, ja que l'efecte dels agents anestèsics i analgèsics és contrarestat pels estímuls nociceptius. Els monitors de profunditat anestèsica, basats en l'estudi dels electroencefalograma, han estat introduïts de forma progressiva en les operacions diàries per proporcionar informació addicional de l'estat del pacient. Tot i això, la quantificació anestèsica encara és un problema sense resoldre.

En aquest projecte, s'ha desenvolupat i aplicat una metodologia basada en algoritmes que empren tècniques de dinàmica simbòlica aplicades al processat de senyals electroencefalogràfiques per tal de predir la resposta d'estímuls nociceptius durant una cirurgia amb sedació i analgèsia. Cal dir que els estímuls, provocats per l'anestesiòleg durant la cirurgia i s'han considerat dins aquest treball, han estat de dos tipus: el RSS (Ramsay Sedation Scale) i el GAG (gag reflex). Aquestes escales per determinar la profunditat anestèsica són models de referència. L'abast del present projecte inclourà: el preprocessat del EEG, el seu posterior processat i l'anàlisi de dites senyals.

La metodologia emprada inclou un preprocessat de la senyal d'EEG, un anàlisi del domini temporal i del freqüencial, el desenvolupament i aplicació de tècniques no-lineals, un anàlisi estadístic i finalment la validació dels resultats. La metodologia basada en dinàmica simbòlica, ja emprada per l'estudi en altres tipus de senyals, s'ha emprat com a tècnica no-lineal. El seu objectiu consisteix en extreure una series de patrons del EEG obtinguts a través de l'aplicació dels dos algoritmes non-lineals proposats.

La dinàmica simbòlica consisteix en la transformació de la senyal temporal en una sèries de símbols al aplicar-hi els algoritmes. D'aquesta sèrie de símbols, es construeixen paraules (patrons) de tres símbols amb un retard d'un símbol, llavors es calcula la probabilitat d'aparició de cadascun dels patrons. Amb tot això, es calculen les entropies de Shannon i Rényi per estimar la complexitat de la distribució de les variables. Tot aquest anàlisi descrit s'ha aplicat a la senyal d'EEG degudament filtrada segons les bandes freqüencials característiques. Els paràmetres involucrats en els algoritmes van ser estadísticament ajustats per tal de caracteritzar d'una millor forma la resposta al estímul nociceptiu. Les variables obtingudes de les metodologies lineals i no-lineals van ser estudiades estadísticament, emprant un test no paramètric i un anàlisi discriminant lineal per avaluar la qualitat de la classificació.

Les noves variables que es proposen en l'actual estudi van ser capaces de descriure els diferents estats amb uns valors: $p\text{-valor} < 6.88\text{E-}6$, $Spe > 60\%$, $Sen > 60\%$ and $P_k > 0.6$. Aquesta metodologia de processat del senyal contribueix tècnicament en la predicció del nivell de profunditat anestèsica durant una cirurgia amb sedació i analgèsia.

ETSEIB

Abstract

The level of sedation in patients undergoing medical procedures evolves continuously since the effect of the anesthetic and analgesic agents is counteracted by noxious stimuli. The monitors of depth of anesthesia, based on the analysis of the electroencephalogram (EEG), have been progressively introduced into the daily practice to provide additional information about the state of the patient. However, the quantification of analgesia still remains an open problem.

In this project, a methodology based on non-linear techniques signal processing algorithms was developed and applied to the electroencephalogram (EEG) for predicting responses to noxious stimulation during Sedation-Analgesia. Two types of stimuli were performed by the anesthesiologist during the surgery sessions, RSS (Ramsay Sedation Scale) and GAG (gag reflex). These sedation scales are considered gold standard. In this work, the scope of the project includes: EEG preprocessing, processing and analysis of the mentioned signals.

The methodology included an EEG signal preprocessing, a time-domain and frequency-domain analysis, the development and application of non-linear techniques, a statistical analysis and finally the validation of the results. Symbolic dynamics methodology, already applied to other kind of signals, was used as a non-linear technique. The aim was to extract a set of patterns from the EEG obtained through two proposed non-linear algorithms.

The symbolic dynamics consists of the transformation of the time signal in a series of symbols by an algorithm. From these new series, words of three symbols were constructed with one symbol delay and their occurrence probability was evaluated in the signals variables. Base on this, the Shannon and Rényi entropies were applied to estimate the complexity of the distribution of the variables. Moreover, thresholds on probabilities were used to construct new variables. The analysis was applied to the EEG filtered according to the characteristic frequency bands (EEG rhythms). The parameters involved in the algorithms were statistically adjusted in order to better characterize the nociceptive response. Variables obtained from linear and non-linear methodologies were submitted to a statistical analysis using a non-parametric test and a linear discriminant analyses to assess the quality of the classification. The leaving-one-out method was used as validation criteria.

New defined variables were able to describe the different states with *p-value* < 6.88E-6, $Spe > 60\%$, $Sen > 60\%$ and $P_k > 0.6$. This signal processing methodology technically contributes to the prediction of anesthesia depth level during Sedation-Analgesia.

Table of Contents

Nomenclature

BIS: Bispectral Index

AAI: A-Line Arx index

Ce_{propo}: Concentration of propofol

Ce_{remi}: Concentration of remifentanil

SD: Standard deviation

PSD: Power Spectral Density

EEG: Electroencephalogram

ECG: Electrocardiogram

EMG: Electromyogram

EOG: Electrooculogram

FFT: Fast Fourier Transform

P_k: Prediction probability

RSS: Ramsay Sedation Scale

GAG: gag reflex

AUC: Area under curve

EQ: equidistant analysis

NEQ: non-equidistant analysis

CNS: Central Nervous System

List of Figures

List of Tables

Chapter 1

Introduction

1.1. General aspects

Conscious sedation is a combination of medicines to help you relax and to block the pain (an anesthetic) during a medical or dental procedure. The level of sedation in patients undergoing medical procedures increases gradually, that is to say, the pain is continuously mitigated with the administration of some drugs.

On the one hand, conscious sedation is usually safe and effective for patients who need minor surgery or a procedure to diagnose an illness. On the other hand, if the patient is given too much of the medicine, problems with the breathing may occur.

The monitors of depth anesthesia, based on the analysis of the electroencephalogram (EEG), have been proven to be helpful in providing additional information about the state of the patient. However, the quantification of anesthesia is an open problem that still needs deep exploration.

The electroencephalogram (EEG) was first measured in humans by Hans Berger in 1929. Electrical impulses generated by nerve firings in the brain diffuse through the head and can be measured by electrodes placed on the scalp. The EEG gives a coarse view of neural activity and has been used to non-invasively study cognitive processes and the physiology of the brain. The analysis of EEG data and the extraction of information from this data is a difficult problem. This problem is exacerbated by the introduction of extraneous biologically generated and externally generated signals into the EEG.

1.2. Objectives of the project

The objective of this project is to develop a methodology based on symbolic dynamics applied to EEG signals in order to predict response to noxious stimulations under surgery procedures. This will allow a prospective objective helping anesthesiologists in giving the correct dose of drug to maintain the patient in a deeply anesthetized condition until the surgery has been performed.

1.2.1. Specific objectives

The study of the Electroencephalography, in order to identify the usual magnitude of the signal, how it is recorded and how the artifacts of the signals are taken into account.

The study of the noxious stimuli, how a doctor induces the response in a patient during a minor surgery procedure.

The familiarization of the different techniques already applied to the EEG signals, so that, it is possible to decide in which directions you can pursue the research.

The construction of a well-defined database, in concordance, with anesthesiologist opinion. The design and implementation of EEG preprocessing algorithms.

The application of two different algorithms based on symbolic dynamics, to define non-linear variables able to predict response to noxious stimulation. The variables types are taken from: time-domain, frequency-domain and non-linear techniques.

The study of the parameters involved in the algorithms to better describe the behavior of the sedation states.

The discriminant statistical analysis, conducted with both MATLAB and SPSS, of the defined variables to differentiate the responsive states, that is to say, these parameters will permit to classify the depth of anesthesia along the recording in the most excellent way.

The multivariable functions analysis to create a new set of variables that can better discriminate the responsive states.

The validation of the proposed variables.

1.3. Scope of the project

Next paragraph is a discussion on some important topics that need to be considered to define the project.

The present work which is framed within the working guidelines set out in the investigation project MICINN (TEC2010-20886-C02-01) of the B2SLab group of the Universitat Politècnica de Catalunya (UPC). In this project, biomedical signal processing techniques based on non-linear dynamics are developed to properly perform a deep of anesthesia evaluation, in line with the National Scientific, Development and Technological Innovation Plan. To this end, in this present thesis it is proposed to use symbolic dynamics techniques applied to study the electroencephalographic signals.

Chapter 2

State of the art

2.1. Origin of the project

A correct evaluation of the depth of anesthesia is especially important in good and useful handling of the patient, both to decrease the incident of awareness in anesthesia and to prevent delays in the recovery phase. Moreover, it is also necessary delivering an adequate amount of drug to the patient, trying to achieve loss of consciousness while maintaining hemodynamic stability and keeping the recovery period short. For all this reasons it is essential to find an accurate method that permits to know exactly in which condition the patient is.

Over the last several decades, investigation has focused on finding reliable noninvasive ways of monitoring DOA (Depth of Anesthesia). Given the highly complex nature of a biological signal, as the electroencephalogram, linear methods are not able to characterize it in a proper way. The researchers, so, have turned attention to the field of non-linear analysis, getting better results.

2.2. Motivation

The aggression that occurs on patient undergoing surgery triggers a series of responses in the body and in the tissue that may have implications on the outcome of the surgical process. To mitigate the intensity of these responses, a certain level of protection or "anesthetic state" must be achieved. The anesthetic state may be defined as the combination of pharmacological effects that minimize the impact of surgical aggression in the patient.

Over the past 40 years, the assessment of depth of anesthesia has been a constantly evolving topic, with the introduction of newer drugs with more specific pharmacological actions. In the [1] editorial, it is reexamined this issue and stated that depth of anesthesia is difficult to define because anesthetists have approached the issue in terms of the drugs available to them rather than the patient's need during surgery.

Inhalational anesthetic depth has been classically characterized by the minimum alveolar concentration (MAC) [2]. The measurement of MAC has several important elements, including 1) a constant partial pressure of volatile anesthetic at the site of action before measurement of response, 2) the application

of a specific noxious stimuli (initial skin incision), and 3) requirement for observation of a defined clinical response, usually purposed movement.

Unfortunately, similar unifying methodology or concepts to sees drug concentration versus depth of anesthesia have not evolved so far for the intravenous anesthetics such as thiopental, methohexital, or propofol. For several years, various methods have been developed for the noninvasive assessment of the level of consciousness during general anesthesia [3-7]. Since the main action of anesthetic agents occurs in the brain, a reasonable choice is to monitor the electroencephalographic signal (EEG). Changes on the EEG signal are directly related to biochemical variations of a drug induced in the brain and the effects on individual behavior. The electroencephalogram (EEG) has been shown to change with sleep, [8] sedation, [9–11] and general anesthesia. [12,13] Different anesthetic and analgesic drugs alter the EEG in a drug-specific fashion. [9,11,14,15] For this reason, it is difficult to give a precise interpretation of EEG changes for assessing depth of anesthesia or sedation when a combination of anesthetic and analgesic drugs has been administered. According to various methods, different EEG monitors have been developed. The three most important monitors consider bispectrum (BIS, A-2000 monitor, Aspect Medical, USA) [15,16], entropy (SE and RE – State and Response Entropy, S/5 Entropy Module, GE Healthcare, Finland) [17] and auditory evoked potentials (AAI, AEP Monitor/2, Danmeter, Denmark) [18,19] whereas the most recent is the qCON (Quantium Medical, Spain) [20].

To overcome the difficulties associated with conventional EEG monitoring, it may also be interesting to evaluate computerized EEG-derived parameters (e.g., power bands: alpha, beta, delta and theta), temporal variables (SD), frequency variables (PSD) and phase-coupling (bispectral index, BIS).

2.3. Prior requirements

The use of processed electroencephalography (EEG) using a simple frontal lead system has been made available for assessing the impact of anesthetic medications during surgery. The foundations of anesthesia monitoring rest on the observations of Guedel with ether that the depth of anesthesia relates to the cortical, brainstem and spinal effects of the anesthetic agents. Anesthesiologists strive to have a patient who is immobile, is unconscious, and stable and who has no intraoperative awareness or recall. These anesthetic management principles apply today, despite the absence of ether from the available anesthetic medications. The use of the EEG as a supplement to the usual monitoring techniques rests on the observation that anesthetic medications all alter the synaptic function which produces the EEG.

Frontal EEG can be viewed as a surrogate for the drug effects on the entire central nervous system (CNS). Using mathematical processing techniques, commercial EEG devices create an index usually between 0 and 100 to characterize this drug effect. Critical aspects of memory formation occur in the frontal lobes making EEG monitoring in this area a possible method to assess risk of recall. Integration of processed EEG monitoring into anesthetic management is evolving and its ability to characterize all

of the anesthetic effects on the CNS (in particular awareness and recall) and improve decision making is under study.

2.4. The nervous system

The nervous system gathers, controls, communicates and process information from various parts of the body, assuring that both internal and external changes are handled rapidly and accurately. The nervous system is unique in the complexity of the control actions that it can perform and is commonly divided into the central nervous system (CNS), consisting of the brain and spinal cord, and peripheral nervous system (PNS), that connect the brain and the spinal cord to organs and sensory system. The two systems are closely integrated: the CNS processes the information received from the PNS sensory input and, way back by the PNS, the brain sends responses to organs or sensory system.

2.4.1. The central nervous system

The human central nervous system can be divided into three major levels with specific functional attributes: the spinal cord level, the lower brain level and the higher brain or cortical level.

In common knowledge the spinal cord level is the conduit for signals from the periphery of the body to the brain or in the opposite direction, from the brain back to the body. However, this is far from the truth because the spinal cord level can attempt other significant tasks that not required signals to reach the cortical level of the brain, such as reflexes that withdraw portion of the body from objects. Other tasks referred to control of local blood vessel and gastrointestinal movements. The upper levels of the central nervous system often operate not by sending signals directly to the body but commanding the centers of the cord to perform the function.

Many of the subconscious activities of the body are controlled in the lower areas of the brain - medulla, pons, mesencephalon, hypothalamus, thalamus, cerebellum and basal ganglia. Each of the subconscious activities such as control of arterial pressure, respiration, control of equilibrium, salivation on response to the taste of food, interests a different area in the lower brain.

The cerebral cortex is the most important part of the CNS and the different regions of cortex are responsible of sensation, learning, voluntary movement, speech and perception. Moreover, the higher brain is an extremely large memory storehouse. The storage of information is the process called *memory* and this is a function of the synapses too. That is the reason why the functions of cortical level are the most complex to explain. The cortical level never functions alone but in association with the lower centers of the nervous system. Without the cerebral cortex the functions of the lower brain are often very imprecise. The information in the cortical part of the brain converts these functions to very determinative and precise operations. Another essential task developed by the cerebral cortex is to processes most of our thought even though it cannot perform this alone.

2.4.2. Neurons

The basic functional unit of the nervous system is the nerve cell – the neuron – which communicates information to and from the brain. All nerve cells are collectively referred to as neurons although their size, shape and functionality may differ widely. Neurons can be classified into groups depending on their functionality morphology or functionality. Using the later classification scheme, three types of neurons can be defined: *sensory neurons*, connected with sensory receptors – visual, auditory tacticle and other kinds -, *motor neurons*, related to control bodily activities – contraction of smooth muscles in the internal organs and secretion by both exocrine and endocrine glands in many parts of the body – and *interneurons*, connected to other neurons.

The Figure 2.1 illustrates a typical neuron structure which consists of three major parts: the *soma*, which is the main body of the neuron and from which extend the other two types of structures, the *dendrites* and the *axon*. The axon extends from the soma to the peripheral nerve. It is usually a single branch which transmits the output signal of the neuron into various parts of the nervous system. The axon is covered by the myelin sheath that enables action potentials to travel faster. The length of the axon varies widely from less than 1mm up to 1 m of the longer axons which run from the spinal cord to the feet. The dendrites consist of as many several thousand projections of the soma, which receive a signal from other neurons. The dendrites extend up to 1 mm in the surrounding areas of the cord.
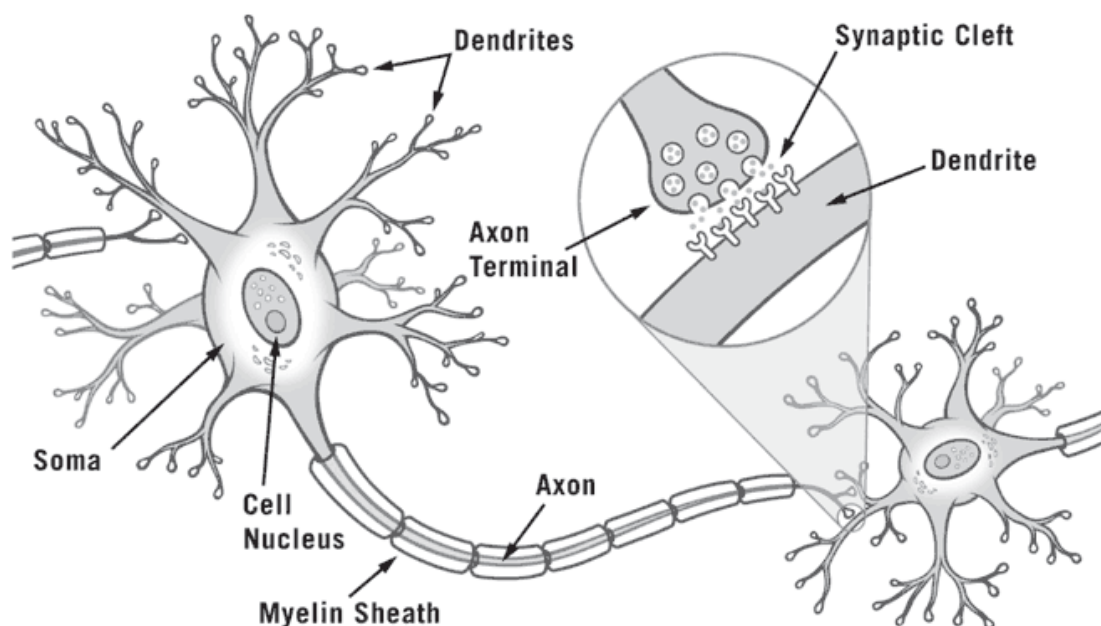
Fig. 2.1. Neuron diagram adapted from internet.

2.4.3. The synapse

The information transmission from one neuron to another takes place at *a synapse* that is the junction point made by the contact between a neuron and the next. The connections, known as *presynaptic terminals*, lie on the surface of the dendrites and the soma may interest axon as well. These terminals are the ends of nerve fibrils that origins in many other neurons and their function may be *excitatory* or *inhibitory*. The first type of terminals secretes a substance that excites the postsynaptic neuron whereas the others secrete a substance that inhibits the neuron. In addition, it is important to point out that the synapse determines the directions that the signals spread in the nervous system. Some postsynaptic neurons respond with a large number of impulses, while others respond with only a few. Thus, the synapse performs a selective action, often blocking the weak signals while allowing the strong signals to pass, often selecting and amplifying certain weak signals, and often channeling the signal in many different directions rather than in simply one direction.

2.4.4. Synapse and neuron electrical activity

Almost all the synapses utilized for electrical signal transmission in the central nervous system are *chemical* synapse (Fig. 2.2). In these, the signal initiates in the soma and propagates through the axon encoded as a short, pulsed waveform. In the presynaptic terminal the signal is converted to a chemical signal. The first neuron secrete a chemical substance called *neurotransmitter* at the synapse, and this transmitter in turn acts on receptors proteins in the membrane of the next neuron to excite the neuron or inhibit it or to modify its sensitivity. The neurotransmitter diffuses across the synaptic gap and subsequently is reconverted to an electrical signal in the postsynaptic neuron. Over 30 transmitter substances have been discovered up to now.
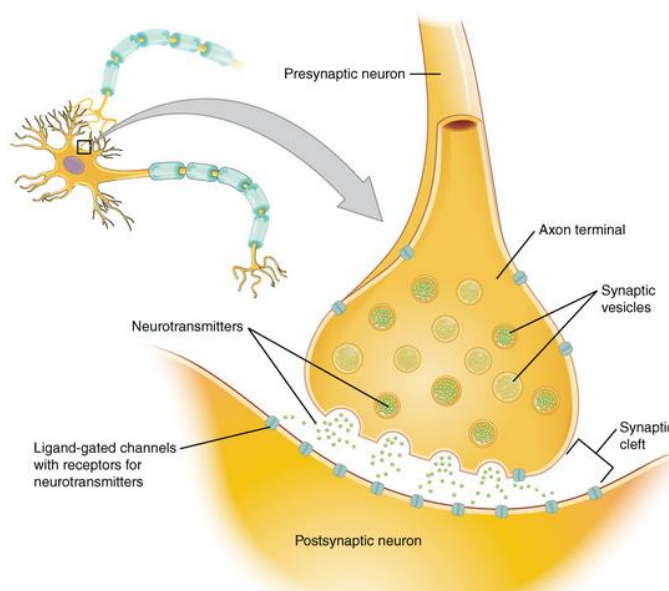
Fig. 2.2. Chemical synapse diagram adapted from internet.

Summation of the many signals received from the synaptic inputs is performed into the postsynaptic neuron. The amplitude of the summed signal depends on the total number of inputs signal and how closely these signals occur in time. The amplitude decreases when the signals become increasingly dispersed in time. The amplitude of the summed signal must exceed a certain threshold to make the neuron fire an action potential. The inhibitory effects do not contribute positively to the excitation. Thus, the output signal of a postsynaptic neuron depends on how the input excitatory and inhibitory signals, received from the wide number of synapse, are summed together. This input/output operation is said to represent one neural computation and is performed repeatedly in billions of neurons.

2.5. Electroencephalography

The cortex, the most important part of the CNS, is the outermost layer of the cerebrum and has a thickness of 2-3 mm. The cortical surface is highly convoluted by ridges and valleys of varying size in order to increase the neuronal area. The area is as large as 2.5 m^2 and includes more than 10 billions of neurons. The collective electrical activity of all the neurons in the cortex level generates a signal which is usually referred to as a *rhythm* because his oscillatory and repetitive behavior. The joint activity of cortical neurons, at a depth down to several millimeters, produces an electrical field which is sufficient strong to be measured in the scalp. The electrical field is mainly generated by currents that flow during synaptic excitation of the dendrites, the excitatory *postsynaptic potentials*.

The functions of the brain are associated with the generation of electrical activity showing a time-varying, oscillating behavior of the brain waves and differing in shape from location to location in the scalp. Moreover, the brain waves differ not only between healthy subjects and subjects with neurological disease, but that the waves are equally dependent on the mental state of the subject – attention, relaxation and sleep – during the recording.

Electroencephalography is an important noninvasive tool in better understanding the human brain and for diagnosing the brain disturbances. The clinical interpretation of EEG has evolved into a discipline up to now but the detection of a biological or mathematical model that fully explains the diversity of EEG patterns remains a challenge.

2.5.1. EEG characteristics: amplitude and frequency.

The Electroencephalogram (EEG) monitors the electrical activity caused by the firing of cortical neurons across the brain's surface. In 1924, German neurologist Hans Berger measured these electrical signals in the human brain for the first time and provided the first systematic description of what he called the Electroencephalogram (EEG). In his research, Berger noticed spontaneous oscillations in the EEG signals (Rosenboom 1999) and identified rhythmic changes that varied as the subject shifted his or her state of consciousness. These variations, which would later be given the name of alpha waves,

were originally known as Berger rhythms (Berger 1929, 355; Gloor 1969; Adrian and Matthews 1934).

Brainwaves are an extremely complex signal. In surface EEG monitoring, any given electrode picks up waves pertaining to a large number of firing neurons, each with different characteristics indicating different processes in the brain. The resulting large amount of data that represents brain activity creates a difficult job for physicians and researchers attempting to extract meaningful information.

Brainwaves have been categorized into four basic groups or bands of activity related to frequency content (0-50 Hz) in the signals: Alpha, Beta, Theta and Delta (Lusted and Knapp 1996). Fig. 2.3 shows each of the frequency bands as displayed by an EEG monitoring system. The electroencephalogram (EEG) is a recording of the electrical activity of the brain from the scalp. The recorded waveforms reflect the cortical electrical activity. The EEG signal intensity is quite small (20-200 μV), measured in microvolts (μV).
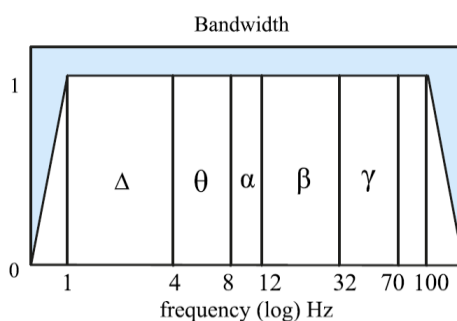
Fig. 2.3. Wideband EEG measurements, adapted from the internet.

The main frequencies of the human EEG waves are (Fig. 2.4):

Delta rhythm: has a frequency of 0.1 to 4 Hz or below. It tends to be the highest in amplitude and the slowest waves. It is normal as the dominant rhythm in infants up to one year and in stages 3 and 4 of sleep. It may occur focally with subcortical lesions and in general distribution with diffuse lesions, metabolic encephalopathy hydrocephalus or deep midline lesions. It is usually most prominent frontally in adults (e.g. FIRDA - Frontal Intermittent Rhythmic Delta) and posteriorly in children e.g. OIRDA - Occipital Intermittent Rhythmic Delta).

Theta rhythm: has a frequency of 4 to 8 Hz and is classified as "slow" activity. It is perfectly normal in children up to 13 years and in sleep but abnormal in awake adults. It can be seen as a manifestation of focal subcortical lesions; it can also be seen in generalized distribution in diffuse disorders such as metabolic encephalopathy or some instances of hydrocephalus.

Alpha rhythm: has a frequency between 8 and 12 Hz. Is usually best seen in the posterior regions of the head on each side, being higher in amplitude on the dominant side. It appears when closing the

eyes and relaxing, and disappears when opening the eyes or alerting by any mechanism (thinking, calculating). It is the major rhythm seen in normal relaxed adults. It is present during most of life especially after the thirteenth year.

Beta rhythm: beta activity is "fast" activity. It has a frequency of 12 to 30 Hz. It is usually seen on both sides in symmetrical distribution and is most evident frontally. It is accentuated by sedative-hypnotic drugs especially the benzodiazepines and the barbiturates. It may be absent or reduced in areas of cortical damage. It is generally regarded as a normal rhythm. It is the dominant rhythm in patients who are alert or anxious or have their eyes open.
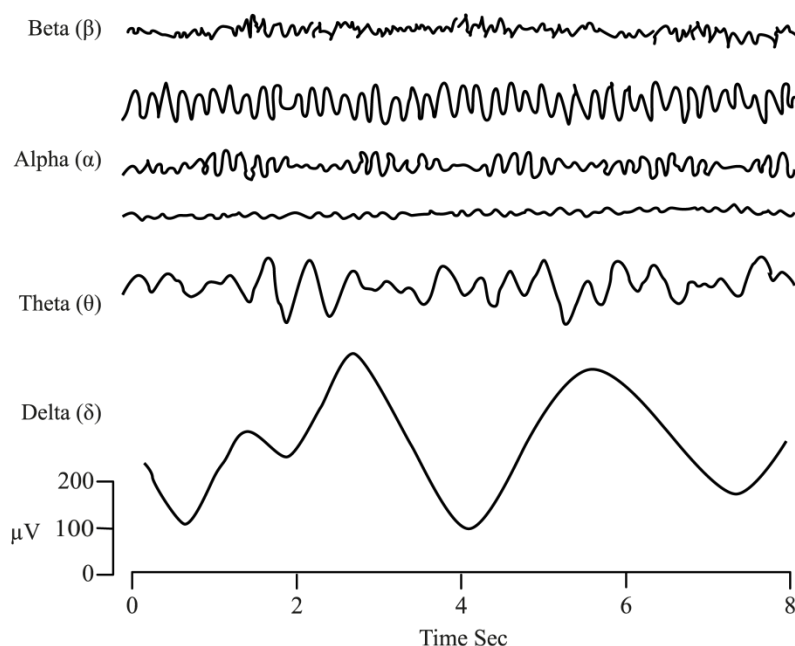
Fig. 2.4. Frequency bands of the EEG, adapted from the internet.

2.5.2. EEG recordings

The EEG recording electrodes and their proper function are crucial for acquiring high-quality data. Different types of electrodes are often used in the EEG recording systems, such as:

- Disposable (gel-less, and pre-gelled types).
- Reusable disc electrodes (gold, silver, stainless steel, or tin).
- Headbands and electrode caps.
- Saline-based electrodes.
- Needle electrodes.

For multichannel recordings with a large number of electrodes, electrode caps are often used. Commonly used scalp electrodes consist of Ag-AgCl disks, less than 3 mm in diameter, with long

flexible leads that can be plugged into an amplifier. Needle electrodes are those that have to be implemented under the skull with minimal invasive operations. High impedance between the cortex and the electrodes as well as the electrodes with high impedances can lead to distortion, which can even mask the actual EEG signals. Commercial EEG recording systems are often equipped with impedances monitors. To enable a satisfactory recording the electrode impedances should read less than 5 kΩ and be balanced to within 1 kΩ of each other. For more accurate measurement the impedances are checked after each trial.

Due to the layered and spiral structure of the brain, however, distribution of the potentials over the scalp (or cortex) is not uniform. This may affect some of the results of source localization using the EEG signals.
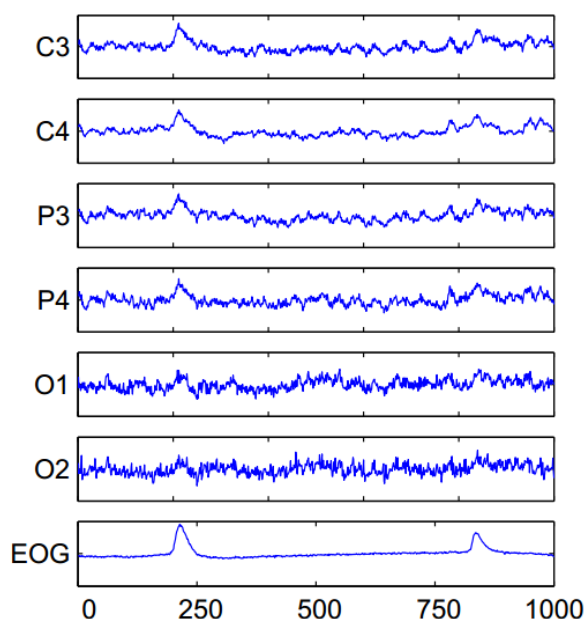
Fig. 3.5. EEG signals recorded in seven different sites.

Fig. 3.5 shows an example of four seconds of EEG data recorded at 250 samples per second from seven sites. The two spikes are the effect of eye blinks on the recorded data. The electrical fluctuations caused by brain activity and recorded as EEG are generally in the range of -50 to 50 microvolts, µV . Eye blinks have a higher amplitude and often have voltages of over 100 µV. Electrodes are labeled according to the International 10-20 system shown in Fig. 2.6.

2.5.3. Conventional Electrode Positioning

The International Federation of Societies for Electroencephalography and Clinical Neurophysiology has recommended the conventional setting (also called 10-20) for 21 electrodes (excluding the earlobe electrodes), as depicted in Fig. 2.6 (A) and Fig. 2.6 (B). Often the earlobe electrodes called A1 and A2, connected respectively to the left and right earlobes, are used as reference electrodes. The 10-20

systems avoids both eyeball placement and considers some constant distances by using specific anatomic landmarks from which the measurement would be made and then uses 10 or 20% of the specified distance as the electrode interval. The odd electrodes are on the left and the even ones on the right.

For setting a larger number of electrodes using the above conventional system, the rest of the electrodes are placed in between the above electrodes with equidistance between them. For example, C_1 is placed between C_3 and C_2. Fig. 2.6 (C) represents a larger setting for 75 electrodes including the reference based on the guidelines by the American EEG Society. Extra electrodes are sometimes used for the measurement of the electrooculogram (EOG), electrocardiogram (ECG), and electromyogram (EMG) of the eyelid and eye surrounding muscles. In some applications such as event-related potential (ERP) analysis and brain computer interfacing a single channel may be used. In such applications, however, the position of the corresponding electrode has to be well determined.

.
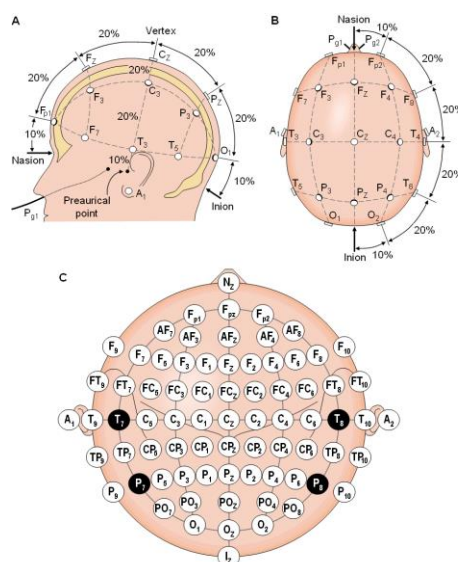
Fig. 2.6. A diagrammatic representation of 10-20 electrode settings for 75 electrodes including the reference electrodes, reproduced from Sharbrough *et al*., 1991: (A) and (B) represent the three-dimensional measures, and (C) indicates a two-dimensional view of the electrode setup configuration.

Two different modes of recording, namely differential and referential, are used. In the differential mode two inputs to each differential amplifier are from two electrodes. In the referential mode, on the other hand, one or two reference electrodes are used. Several different reference electrode placements can be found in the literature. Physical references can be used as vertex (C_z), lined-ears, linked-mastoids, ipsilateral ear, contralateral ear, C_7, bipolar references, and tip of the nose. There are also reference-free recording techniques, which actually use a common average reference. The choice of reference may produce topographic distortion if the reference is not relatively neutral. In modern instrumentation, however, the choice of a reference does not play an important role in the

measurement. In such systems other references such as FP_z, hand, or leg electrodes may be used. The overall setting includes the active electrodes and the references.

In many applications such as brain-computer interfacing (BCI) and study of mental activity, often number of electrodes around the movement-related regions are selected and used from the 10-20 setting system.

2.5.4. Artifacts in electroencephalography

Contamination of EEG data can occur at many points during the recording process. Most of the artifacts considered here are biologically generated by sources external to the brain. Improving technology can decrease externally generated artifacts, such as line noise, but biological artifact signals must be removed after the recoding process. Fig. 2.7 shows waveforms of some of the most common EEG artifacts, each of which is discussed below. (Knight J.N., 2003)
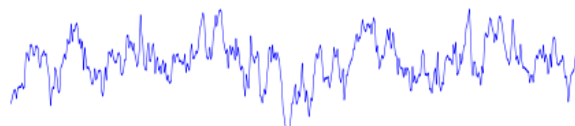
Fig. 2.7. Clean EEG signal.

Eye Blink. The eye blink artifact is very common in EEG data. It produces a high amplitude signal that can be many times greater than the EEG signals of interest (see Fig. 2.8). Because of its high amplitude an eye blink can corrupt data on all electrodes, even those at the back of the head (See Figure 2.6). Eye artifacts are often measured more directly in the EOG, pairs of electrodes placed above and around the eyes. Unfortunately, these measurements are contaminated with EEG signals of interest and so simple subtraction is not a removal option even if an exact model of EOG diffusion across the scalp is available.
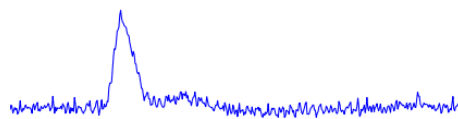
Fig. 2.8. Eye blink signal.

Eye Movement. Eye movement artifacts (see Fig. 2.9) are caused by the reorientation of the retinocorneal dipole [21, 22]. This artifact's diffusion across the scalp is stronger than that of the eye blink artifact. Eye blinks and movements often occur at close intervals producing an effect shown in Fig. 2.10.
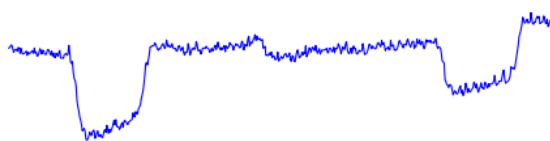
Fig. 2.9. Eye movement signal.
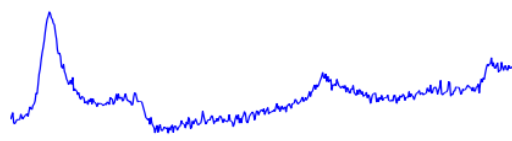
Fig. 2.10. Overlap of eye blink and eye movement artifacts.

Line Noise. Strong signals from A/C power supplies (see Fig. 2.11) can corrupt EEG data as it is transferred from the scalp electrodes to the recording device. This artifact is often filtered by notch filters, but for lower frequency line noise and harmonics this is often undesirable. If the line noise or harmonics occur in frequency bands of interest they interfere with EEG that occurs in the same band [21]. Notch filtering at these frequencies can remove useful information. Line noise can corrupt the data from some or all of the electrodes depending on the source of the problem.
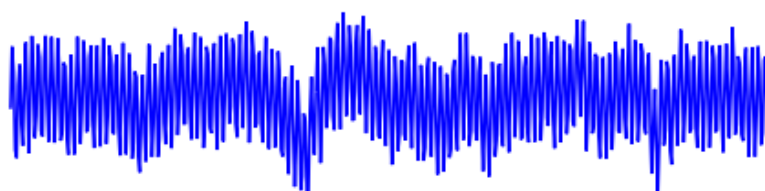
Fig. 2.11. Example of a 60 Hz line noise.

Pulse. The pulse, or heart beat, artifact (see Fig. 2.12) occurs when an electrode is placed on or near a blood vessel. The expansion and contraction of the vessel introduce voltage changes into the recordings. The artifact signal has a frequency near 1.2Hz, but can vary with the state of the patient. This artifact can appear as a sharp spike or smooth wave [23].

Fig. 2.12. Example of a pulse signal.

2.6. Sedation-Analgesia

2.6.1. Nociception

Nociception is the encoding and processing of harmful stimuli in the nervous system [24], and, therefore, the ability of a body to sense potential harm. It is the afferent activity in the peripheral and central nervous systems produced by stimulation of specialized free nerve endings called "nociceptors" or "pain receptors" that only respond to tissue damage caused by intense chemical (e.g., chilli powder

in the eyes), mechanical (e.g., pinching, crushing) or thermal (heat and cold) stimulation.[25][26] Once stimulated, a nociceptor sends a signal along a chain of nerve fibers via the spinal cord to the brain. Nociception triggers a variety of autonomic responses and may also result in a subjective experience of pain in sentient beings. [26]Nociceptive neurons generate trains of action potentials in response to intense stimuli, and the frequency of firing determines the intensity of the pain.[27]

The three types of pain receptors are cutaneous (skin), somatic (joints and bones), and visceral (body organs). It was previously believed that pain was simply the overloading of sensory receptors, but research in the first half of the 20th century indicated that pain is a distinct phenomenon that intertwines with all of the other senses, including touch. Pain was once considered a non-material experience, but recent studies show that pain is registered in specific parts of the brain. The main function of pain is to attract our attention to dangers and motivate us to avoid them.

2.6.2. Detection of noxious stimuli

Potentially damaging mechanical, thermal, and chemical stimuli are detected by nerve endings called nociceptors, which are found in the skin, joint surfaces, and in some internal organs. The concentration of nociceptors varies throughout the body; they are found in greater numbers in the skin than in deep internal surfaces. The nociceptors are unspecialized free nerve endings that have their cell bodies outside the spinal column in the dorsal root ganglia.[28]

Nociceptors have a certain threshold, that is, they require a minimum intensity of stimulation before they trigger a signal. Once this threshold is reached a signal is passed along the axon of the neuron into the spinal cord.

The perception of noxious stimuli (termed nociception by Sherrington) is not the same thing as pain, which is a subjective experience and includes a strong emotional (affective) component. The amount of pain that a particular stimulus produces depends on many factors other than the stimulus itself. A stabbing sensation in the chest will cause much more pain if it occurs spontaneously in a middle-aged man than if it is due to a 2-year-old poking him in the ribs with a sharp stick. The nociceptive component may be much the same, but the affective component is quite different.

2.6.3. Nociceptive afferent neurons

In the nervous system, afferent neurons (otherwise known as sensory, receptor neurons and afferent fibers) carry nerve impulses from receptors or sense organs toward the central nervous system. Afferent neurons communicate with specialized interneurons. The opposite activity of direction or flow is efferent.

Under normal conditions, pain is associated with impulse activity in small-diameter primary afferent fibres of peripheral nerves (see Raja *et al.*, 1999). These nerves have sensory endings in peripheral tissues and are activated by stimuli of various kinds (mechanical, thermal, chemical; Julius &

Basbaum, 2001; Julius & McCleskey, 2006). They are distinguished from other sorts of mechanical and thermal receptors by their higher threshold, because they are normally activated only by stimuli of noxious intensity-sufficient to cause some degree of tissue damage. Recordings of activity in single afferent fibers in human subjects have shown that stimuli sufficient to excite these small afferent fibres also evoke a painful sensation. Many of these fibres are non-myelinated C fibres with low conduction velocities (< 1 m/s); this group is known as C polymodal nociceptors. Others are fine myelinated (Aδ) fibres, which conduct more rapidly but respond to similar peripheral stimuli. Afferents from muscle and viscera also convey nociceptive information. In the nerves from these tissues, the small myelinated Aδ fibres (Fig. 2.13) are connected to high-threshold mechanoreceptors, while the non-myelinated C fibres are connected to polymodal nociceptors, as in the skin.

Experiments on human subjects, in which recording or stimulating electrodes are applied to cutaneous sensory nerves, have shown that activity in the Aδ fibres causes a sensation of sharp, well-localised pain, whereas C fibre activity causes a dull, diffuse, burning pain.
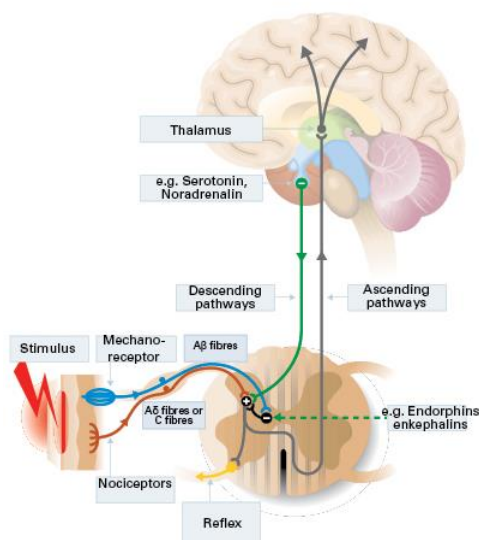
Fig. 2.13. Diagram representing the nociceptive system.

Pain is a disabling accompaniment of many medical conditions, and pain control is one of the most important therapeutic priorities. The following subsection discusses how drugs are used to reduce the neural mechanisms responsible for different types of pain. During surgery, the anesthesiologist must administrate an anesthetic drug to lose consciousness (propofol) and an analgesic drug to mitigate the pain suffered (remifentanil). The effects caused by these two drugs are discussed below.

2.6.4. Sedation and anesthesia

The definitions of sedation and anesthesia are referring to the patient's level of awareness and response to stimulation. The term "sedation" comes from the Latin word sedare, meaning "to settle", "to calm".

The term "anesthesia" comes from the Greek word anaisthesia, meaning "lack of sensation", "loss of feeling" (Harper, 2001).

The term sedation is used when a patient in the intensive care unit, for example, is given a small dose of anesthetic drug to make him/her calm and minimize the anxiety.

Sedation is further divided into two subcategories:

- **Light sedation**: is the state where the level of consciousness is minimally suppressed, and the patient is able to breathe independently and to respond appropriately to verbal command or physical stimulation.
- **Deep sedation**: is the state of moderately suppressed consciousness or of the unconsciousness, the protective reflexes, i.e independent breathing and responses to verbal or physical stimuli, are not preserved (Murphy, 1996).

The depth of sedation can be clinically assessed by using the Ramsay score, which is used in this thesis to study the differences between the two state of awake and sedated.

Anesthesia: is defined as the state of unconsciousness, amnesia and hemodynamic, motor, and endocrinologic stability during surgery, produced by specific medication (van Gils, 2002). This means that for achieving an adequate level of anesthesia, usually a combination of hypnotic, analgesics, and neuromuscular blocking agents are used. Therefore, general anesthesia consists of three partially dependent components. A short description is given subsequently.

Hypnosis: with the use of hypnotic medication the patient is taken to the unconscious state and he is unaware of ongoing events.

Analgesia: Painless is obtained with the use of analgesic medication. Despite the fact that the patient could be in deep hypnosis, his body can still perceive the pain (nociception). Therefore, the purpose of analgesia is to assure antinociception.

Muscle relaxation: The relaxed state of muscles is often required for the surgeon to perform an operation, it is usually obtained either by the use of neuromuscular blocking agents or sufficient combination of hypnosis and analgesia.

2.6.5. Anesthetic effects on the nociceptive pathway

Even the fastest-acting inhalation anesthetics, such as nitrous oxide, take a few minutes to act and cause a period of excitement before anesthesia is produced. Intravenous anesthetics act much more rapidly, producing unconsciousness in about 20 seconds, as soon as the drug reaches the brain from its site of injection. These drugs (e.g. thiopental, etomidate, propofol) are normally used for induction of

anesthesia. They are preferred by patients because injection generally lacks the menacing quality associated with a face mask in an apprehensive individual.

Propofol, introduced in 1983, is also similar in its properties to thiopental, but it has the advantage of being very rapidly metabolized and therefore giving rapid recovery without any hangover effect. This enables it to be used as a continuous infusion to maintain surgical anesthesia without the need for any inhalation agent. Propofol drug information lacks the tendency to cause involuntary movement and adrenocortical suppression seen with etomidate. It is particularly useful for day case surgery. In this subsection are listed the most remarkable effects that should be considered during general anesthesia.

- Anesthesia involves three main neurophysiological changes: unconsciousness, loss of response to painful stimulation and loss of reflexes.
- At supra-anesthetic doses, all anesthetic agents can cause death by loss of cardiovascular reflexes and respiratory paralysis.
- At the cellular level, anesthetic agents affect synaptic transmission rather than axonal conduction. The release of excitatory transmitters and the response of the postsynaptic receptors are both inhibited.
- Although all parts of the nervous system are affected by anesthetic agents, the main targets appear to be the thalamus, cortex and hippocampus (brain parts).

2.6.6. Analgesic effects on the nociceptive pathway

Remifentanil is a potent ultra-short-acting synthetic opioid analgesic drug. It is given to patients during surgery to relieve pain and as an adjunct to an anesthetic. Remifentanil is used for sedation as well as combined with other medications for use in general anesthesia. The use of remifentanil has made possible the use of high-dose opioid and low-dose hypnotic anesthesia, due to synergism between remifentanil and various hypnotic drugs and volatile anesthetics.

At the spinal level, remifentanil inhibits transmission of nociceptive impulses through the dorsal horn and suppresses nociceptive spinal reflexes, even in patients with spinal cord transection. There is also evidence (see Sawynok, 2003) that opiates inhibit the discharge of nociceptive afferent terminals in the periphery, particularly under conditions of inflammation, in which the expression of opioid receptors by sensory neurons is increased.

2.6.7. Effects of general anesthesia on sensory processing

Anesthetic drugs influence both the frequency content and the amplitude of the EEG signal. Evaluating in a proper way the DOA is extremely important in good and useful treatment of the patient. [42] However, as the statistical characteristics of biological signals often change with time, and are

typically highly irregular and non-stationary, analyses of such systems are complicated. In fact, none of the parameters used to this aim has satisfactorily described the complexity of the system. Patient hemodynamics like blood pressure, heart rate, tearing and sweating cannot avoid awareness and movement during surgery. Neither plasma nor the effect site concentrations of the drugs are direct measures of clinical effect. Solving this problem, the Central Nervous System, the main target for anesthetic agents, has received a great deal of attention and EEG based methods have been widely used for estimating the anesthetic depth.

The measures of the electroencephalogram taken during anesthesia exhibit stereotypic changes as anesthetic depth increases. These changes include complex patterns of frequency slowing accompanied by amplitude increases which typically peak when loss of consciousness occurs (loss of responses to verbal commands; loss of righting reflex). As anesthetic depth increases from light surgical levels to deep anesthesia, the EEG exhibits disrupted rhythmic waveforms, high amplitude burst suppression activity, and finally, very low amplitude isoelectric or 'flat line' activity.

Various signal analysis approaches have been used to quantify these pattern changes and can provide an indication of loss of recall, loss of consciousness and anesthetic depth. Monitors have been developed using various algorithms for signal analysis and are commercially available, but none have as yet proven 100% accurate.

2.7. State of the art: techniques for detecting the level of sedation

In the fallowing paragraphs the state of art of EEG analysis techniques are presented. Nowadays, due to the chaosity of the EEG signal, most of the methods are based on non-linear techniques of analysis such as the largest Lyapunov exponent, correlation dimension, correlation integral, entropy and time-frequency analysis.

In the following Fig. 2.14, there are interesting recent works related to the topic of sedation and drug administration.

Authors	Anes data set	Feature extraction	Classifier	Results
M. Krkic et al. [3]	Human anes data with different anesthetic drug Group a: inhalation of disflurane Group b: Injection of propofol	Spectral entropy Embedding space eigen spectrum	Radial basis neural network	98±0.2%
Rob. J. Roy et al. 1999 [4]	Anes data recorded from dog Drug used is propofol	Approximate entropy Spectral edge freq Lempel ziv complexity	Adaptive network based fuzzy interference system (ANFIS) Comparison done with AAN	89.5% 89.5%
Rob. J. Roy et al. 2001 [1]	Human anes data (vascular surgery)	Lempel ziv complexity	Under diff anes agents Comparison done with ApEn	93% accuracy with Lempel ziv when compared with ApEn
G. Widman et al. 2000 [10]	Human anes data	Power spectral measures Bispectral index Nonlinear correlation index	–	–
Jin Xu et al. 2004 [18]	Anes data extracted from rats	Lempel ziv complexity	–	Complexity decreases while DOA increases and vice versa
Richard C. Watt et al. [19]	Human anes data (light, normal, deep anesthesia)	Correlation dimension	–	Dimensionality decreases as anesthetic depth increases
Zhang Lianyi et al. 2005 [2]	Human anes data with different diseases like adrenal gland tumor, stomach cancer-fentanyl anes agent	Auto correlation	–	It has been shown that prefontal cortex area on autocorrelation is sensitive to different depths during general anesthesia

Fig. 2.14. Relevant works on anesthetic detection from [29].

2.7.1. Lyapunov exponent based techniques

Iasemidis *et al.* (Iasemidis *et al.* 1990; Iasemidis et al., 2004) conducted their first studies on th temporal evolution of the short-therm largest Lyapunov exponent (LE) for patients with temporal lobe epilepsy. In a *p*-dimensional system there are *p* different Lyapunov exponents, λ_i. They measure the exponential rate of convergence or divergence of the different directions in the phase space. If one of the exponents is positive, the system is chatotic. Thus, two close initial conditions will diverge exponentially in the direction defined by that positive exponent. Since these exponents are ordered, $\lambda_1 \geq \lambda_2 \ldots \geq \lambda_d$, to study the chaotic behavior of a system is sufficient for studying the changes in the largest Lyapunov exponent, λ_1.

The paper [29] discusses an automated detection method of anesthetic depth levels based on EEG recordings using non-linear chaotic features and neural network classifiers. Three non-linear parameters, namely, correlation dimension (CD), Lyapunov exponent (LE) and Hurst exponent (HE) are used as features and two neural network models, namely, multi-layer perception network (feed forward model) and Elman network (feed back model) are used for classification. The neural network models are trained and tested with single and multiple features derived from chaotic parameters and the performances are evaluated in terms of sensitivity, specificity and overall accuracy. It is found

from the experiments results that the Lyapunov exponent feature with Elman network yields an overall accuracy of 99% in detecting the anesthetic depth levels.

2.7.2. Entropy based techniques

Entropy rates are measures designed to quantify the regularity of a time series or the predictability of new values based on previous observations. The complexity of a stochastic process evolving in time can be represented by the rate that the system loses information about previous states. This complexity can be described using entropy rates, which tend to zero for processes with periodic repetition and conversely tend to high values for processes with aperiodic or random behavior.

For a dynamical system evolving in some measurable state space, the entropy rates are related to Kolmogorov-Sinai entropy (KSE). This allows the measurement of entropy rates not only when a time-series is considered as a projection of a trajectory of a dynamical system (e.g. low-dimensional chaotic system) but also when a general linear or non-linear stationary stochastic process is assumed.

Problems arise when entropy rates or KSE [30] has to be estimated from a finite number of observations containing a relatively high noise component - as EEG data under anesthesia.

Geng *et al. also* applied a non-linear dynamic parameter, approximate entropy (ApEn), to EEG time series to evaluate the complexity of the signal (Geng *et al*., 2010). ApEn assigns a non-negative number to a sequence or time series, with a larger values corresponding to a greater apparent process randomness or serial irregularity, and smaller values corresponding to more instances of recognizable features or patterns in the data. ApEn presents some advantages such as need of a lower number of data pints, robustness against noise and wild value point and suitableness for both deterministic and stochastic processes.

2.7.3. Time-frequency techniques

To study the depth of anesthesia on the basis of the EEG, the Choi-Williams distribution (CWD) was used [31] on recordings taken from dogs. The depth of anesthesia has been evaluated by observing the response to a stimulation of the tail. A positive response is regarded as wake state (depth 0) and a negative response as asleep state (depth 1). It has been observed that, for depth 0, the time-frequency contents of the CWD become localized in time and frequency during the period of stimulation and the percentage of energy in the delta and theta bands increases. For depth 1, the time-frequency contents of the CWD remain unchanged during the stimulation period.

2.7.4. Autoregressive Models

One of the most important problems in EEG analysis is the extraction of features to describe EEG signals, because the power of any EEG analysis method depends on the quality of the chosen features (lopes da Silva, 1987). The classification procedure of the Narkograph works to date with with widely

used spectral parameters as EEG describing features. As in some papers of late years (Blinowska *et al*., 1981; Jansen, Hasman and Visser, 1978; Jansen, Bourne and Ward, 1981; Matthis, Scheffner and Benninger, 1981) the superiority of autoregressive (AR) models promises an improvement of the classification procedure.

In a first study of Bender *et al*. (1991) it was shown that the extraction of AR parameters from EEG periods of 2 seconds and the application of quadratic discriminant analysis (QDA) has advantages in comparison with the former method using spectral parameters. Although the set of AR parameters is smaller than the set of spectral parameters, the classification results are just as good or better. Especially, the frequently confounded stages "awake" and "slight anesthesia" can better be recognized by AR parameters [32].

2.7.5. Bispectral analysis techniques

Bispectral analysis was first introduced by geophysicists in the early 1960s to study ocean wave motion, atmospheric pressure changes, seismic activity, and sunspots [33]. It was applied to EEG signal first by Barnett *et al*. [34] and Dumermuth *et al*. [35] in 1971.

Analysis of EEG is typically performed using Fourier analysis, which is useful for detecting frequency components that correspond to the mental state of a patient. Typically, such information is obtained from the magnitude spectrum, as the information content of the phase spectrum can be harder to interpret.

Although use of the magnitude spectrum is sometimes sufficient, in many instances, the phase information is critically important. Bispectral analysis offers a way of gaining further phase information by detecting phase relationships between frequency components. Such relationships have been shown to exist in a medical context during periods where a patient has an impaired mental state (for example see [36]).

Bispectral analysis makes use of phase information by detecting whether the phase of signal components at frequencies f_1, f_2 and f_3 and interdependent. Furthermore, the degree of dependence is quantified so that a high bispectrum correlates to a signal with highly interdependent frequency components.

Chapter 3

The Analyzed Database

3.1. Database

The database belongs to the Department of Anesthesiology, Hospital Clínic of Barcelona (Spain). This database contains data recorded from 378 patients (247 men, mean age 6323 years) undergoing ultrasonographic endoscopy of the upper gastrointestinal tract under sedation and analgesia with propofol and remifentanil. All the patients belong to 1-3 ASA classification. Patients with altered central nervous system, medicated with analgesics or drugs with central effects on the perception of pain, from moderate to severe cardiomyopathy, neuropathy or hepatopathy that needed control during the anesthetic process were not included in the database. The study received approval from the Ethics Committee of Hospital Clinic de Barcelona and all the patients signed informed consent. For each patient, the following information is available: predicted concentrations of propofol (Ce_{propo}) and remifentanil (Ce_{remi}); bispectral Index (BIS) and electroencephalogram (EEG) signal (Fig. 3.1). The observed categorical responses after applying nociceptive stimuli include the evaluation of the Ramsay Sedation Scale level (RSS) (see Table 3.1) [37] after nail bed compression, and the evaluation of the gag reflex presence during endoscopy tube insertion (GAG).

On the one hand, specifically RSS= {2, 3, 4, 5} corresponds to a patient who responds with purposeful movement after compression while patients nail bed in the RSS={6} category do not respond. The RSS score was evaluated at random times during the procedure to avoid those factors correlated with time, which could confound the results of the RSS measurements. The whole database contains annotated RSS scores from 2 to 6. On the other hand, GAG corresponds to a positive nausea reflex during endoscopy tube insertion, a noxious stimulus as well. The presence and the absence of gag reflex were set to GAG= {1} and GAG={0}, respectively.

The EEG was recorded with a sampling frequency of 900 Hz, with a resolution of 16 bits and a recording time of about 60 min using AEP monitor/2 (Danmeter, Odense, Denmark). A 3-electrode montage was used: middle forehead (+), malar bone (-), and left forehead electrode used as reference. Propofol and remifentanil were infused using a TCI system (FreseniusVial; Chemin de Fer, Béziers, France). All information Ce_{propo}, Ce_{remi}, BIS, RSS and GAG were annotated with a resolution of 1 second.

The traditional bands analysis was performed on EEG signals filtered between 0.1-45 Hz and resampled at 128 Hz. After the resampling process, the EEG signals were segmented in windows of length of 1 minute between 30 s and 90 s before the response annotation of RSS or GAG in order to avoid the effect of the stimulation on the signal. The selected windows were filtered into the following frequency bands: δ, 0.1-4 Hz; θ, 4-8 Hz; α, 8-12 Hz; β, 12-30 Hz; TB (total frequency band); 0.1-45 Hz and ALL Spectrum, 0-45 Hz .

The annotated RSS was assigned to the previous 1 minute length window if the differences ΔCeRemi and ΔCeProp between the first and the last second of the window were ΔCeRemi<0.1 ng/ml and ΔCeProp<0.1 ng/ml. Otherwise, the window was taken till the sample where the conditions were satisfied. Windows of EEG containing high amplitude peak noise were processed with a filter based on the analytic signal envelope (ASEF) [38]. If adjacent samples differ more than 10% of the mean of the previous samples differences, that samples and the subsequent ones were not taken into account. In this way, the smallest window resulted to be of 50s.

Score	Response
1	Anxious or restless or both
2	Cooperative, oriented and tranquil
3	Responding to commands
4	Brisk response to stimulus
5	Sluggish response to stimulus
6	No response to stimulus

Table 3.1. Ramsay Sedation Scale
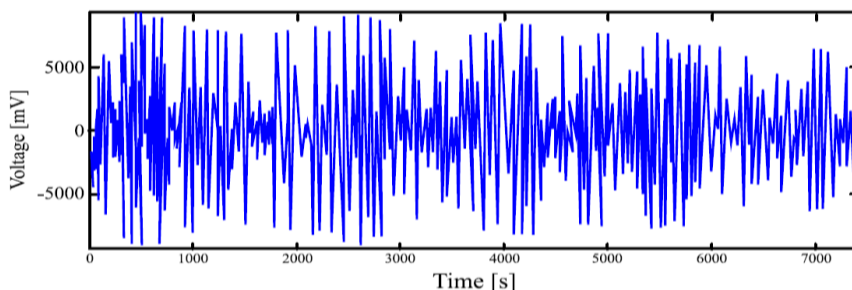
Fig. 3.1. EEG signal of one of the patients of the analyzed database.

General anesthesia

The Target Controlled Infusion (TCI) system administered propofol and remifentanil according to the predictions of pharmacokinetic–pharmacodynamic models. In both cases, the TCI was targeting the effect site, applying the Schnider model for propofol (Ce_{prop}) and the Minto model for remifentanil (Ce_{remi}). The surgeries were ambulatory procedures, including inguinal hernia repair, laparoscopic cholecystectomy, gynecologic laparoscopy and other minor gynecologic procedures. The nociceptive stimulation level was not high, which is usual in this kind of procedures. There were no specific requirements for anesthetic management with regards to preventing movement. It was an observation after stimuli.

Equipment

AEP monitor/2 (Danmeter, Odense, Denmark, Electrodes - Blue Sensor (Medicotest, Olstykke, Denmark), Skin abrasion - One-step skin prep (3M, Ontario, Canada).

Clinical end points

Loss of eyelash reflex was assessed during the transition from awake to anaesthetized, defining the state of LOC. The values for BIS awake were the mean BIS values of -min interval immediately before the infusion pumps were started, while the anaesthetized value was the mean taken over the 1-min interval immediately after LOC.

Movement as a response to laryngeal mask airway (LMA) insertion, laryngoscopy or tracheal intubation was recorded. Movement in the period of 1 min after applying the stimuli was interpreted as the response to each one of the nociceptive stimuli.

3.2. Preprocessing

The preprocessing has to remove the artifacts without losing the main EEG components in order to recover the signal which best represents the brain functioning. As the mixture of EEG and artifact is non-linear, separation of the artifact from the actual signal is very difficult. Among the more significant artifacts are EMG from contracting scalp and facial muscles (Akai, 1999), EOG from eye blinks and saccades (Gratton, 1998). The line noise and other frequency-specific noise can easily be eliminated using filters.

This paragraph deals with the filters used in the preprocessing of the signal. Different types of filter were used in different steps of this study. The Eq. 3.1 of a generic digital filter transfer function is:

$$H(z) = \frac{B(z)}{A(z)} = \frac{b(1) + b(2)z^{-1} + \cdots + b(n+1)z^{-n}}{1 + a(2)z^{-1} + \cdots + a(n+1)z^{-n}} \qquad \text{(Eq. 3.1)}$$

where $A(z)$ and $B(z)$ are respectively the polynomials of the autoregressive and moving average part.

Firstly, a particular filter based on the Hilbert transform was implemented to remove the peaks from the signal. Then, a FIR filter was used to study the traditional frequency bands. All the signal preprocessing operations were conducted using MATLAB.

3.3. The ASEF

EEG signal is very susceptible to a variety of large signal contamination such as power line noise, biological or electrode artifacts. As these artifacts can be associated to cerebral activity they should be removed by filtering before further signal analysis. However, traditional methods, such as band pass filter, are not adequate if the frequency band of the contaminant signal is within the band of the true signal, for example the electromyography signal.

A new methodology to reduce these artifacts was proposed by Melia *et al*. [38] where a filter based on the analytic signal envelope was designed.

The proposed algorithm [38] implements a filter based on Hilbert envelope (HEF) that reduces the amplitude of peaks and spikes in the EEG signals.

The algorithm is based on filtering the envelope $m(t)$ of a signal $x(t)$ with a low pass filter. Furthermore, a threshold $Th(t)$ can be defined on the filteres envelope $m_{filt}(t)$ and applied to the envelope $m(t)$ (see Eq. 3.2). This threshold is calculated for each time sample of $m_{filt}(t)$ as:

$$Th(t) = m_{filt}(t) + k\overline{m_{filt}(t)} \qquad (\text{Eq. } 3.2)$$

where $\overline{m_{filt}(t)}$ is the mean value of $m_{filt}(t)$ and k is an arbitrary constant.

The variable k indicates the filter strength, decreasing the k towards zero means to increase the filter strength. In this work, the analyzed signals were filtered with following values of k: $k = \{0.5, 1, 1.2\}$.

An example of the Hilbert based filter is shown in the Fig. 3.2 where it is possible to notice the difference between the signal before and after the application of the algorithm. This filter decreases the intensity of the signal but keeps the frequency information using the Hilbert transform.
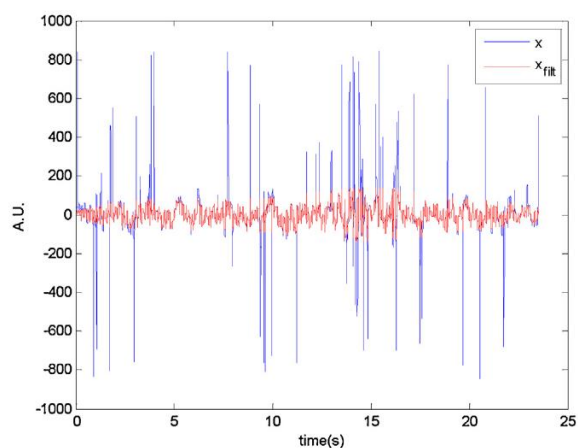
Fig. 3.2. $x(t)$ is a real EEG signal and $x_{fil}(t)$ is the filtered signal using ASEF [38].

3.4. Finite Impulse Response filtering

The second filter applied to the data was a Finite Impulse Response (FIR) filter. The characteristics of the filter were:

- Filter order, $n = 50$.
- Cut-off frequency, $\omega_n = [0.1, 0.4]$ Hz (example of the δ band).
- Sampling frequency, $f_s = 128$ Hz.
- Hammig window.

This Fig. 3.3 is a Hamming-window based, linear-phase filter with normalized cutoff frequency w_n.
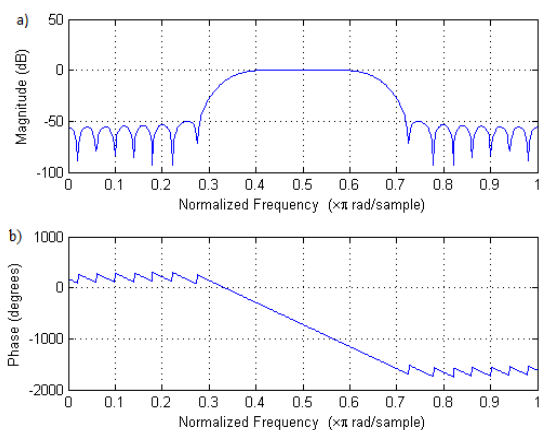
Fig. 3.3. Design a 48th-order FIR bandpass filter with passband of $0.35 \leq \omega \leq 0.65$ [rads/sample].The plots show the characteristics of the Finite Response Filter: (a) magnitude and (b) phase.

Chapter 4

Methodology

4.1. Materials and Methods

This subsection describes research design and data processing techniques. Fig. 4.1 gives an overview.
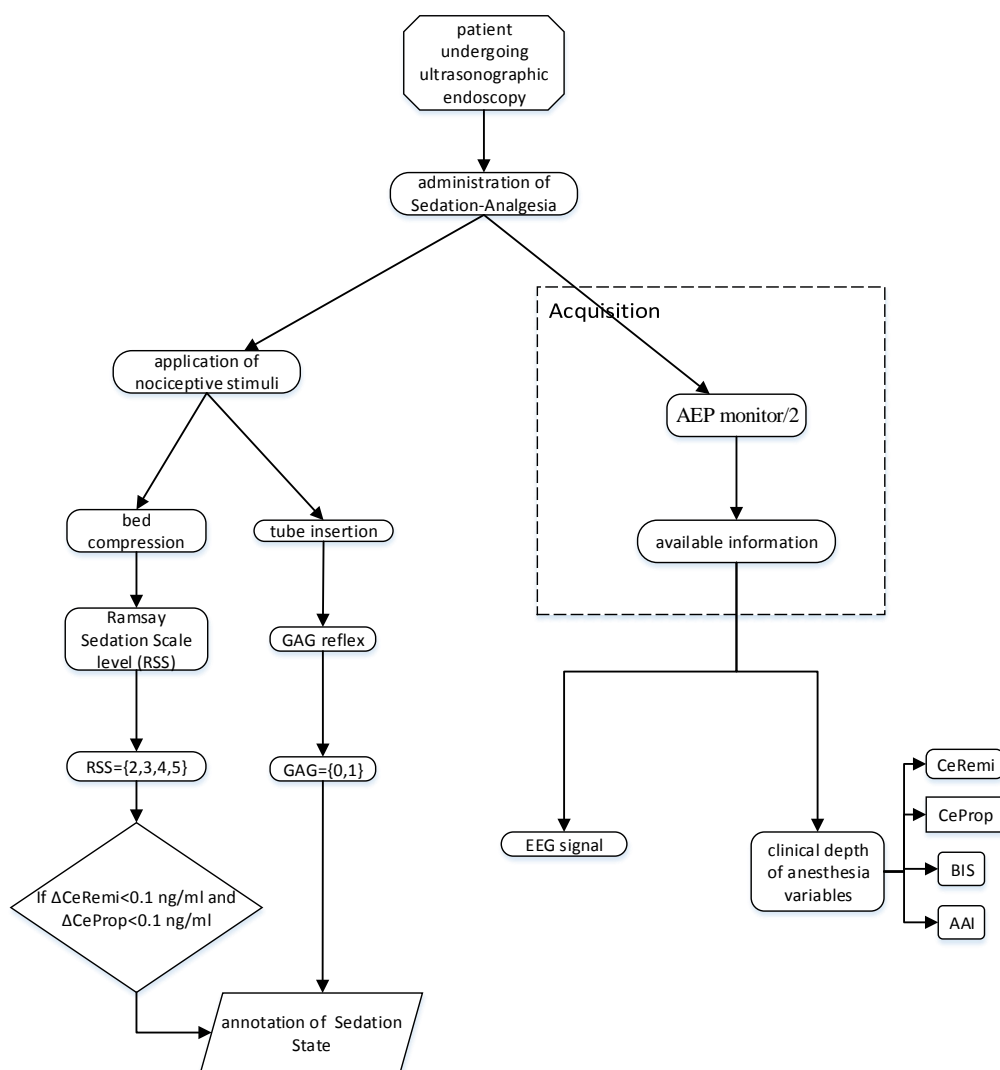
Fig. 4.1. Overview of the data acquisition steps.
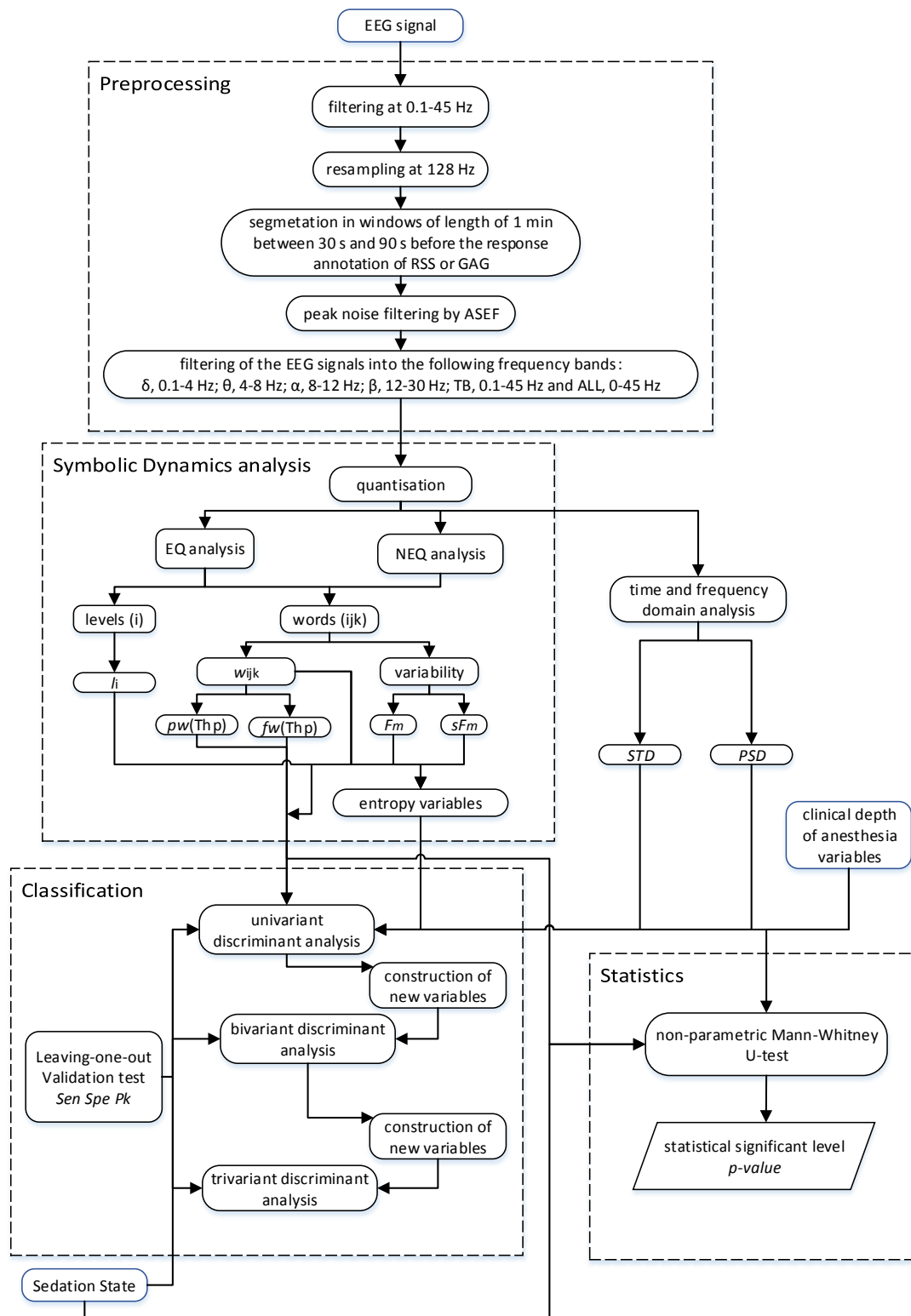
Fig. 4.2. Overview of the preprocessing, processing and classification steps.

4.2. Time-domain analysis

An analysis of the dataset in the time-domain and the frequency-domain was conducted for each passage collected. Each passage contains in the dataset is made of n_z =7.425 samples.

The mean or expected value (see Eq. 4.1) is used to measure the central tendency of a probability distribution. In this study, the mean value of each passage was evaluated as:

$$\bar{x} = \frac{1}{n_z} \sum_{i=1}^{n_z} x_i \qquad \text{(Eq. 4.1)}$$

Similarly, the corrected sample standard deviation (see Eq. 4.2) for each passage was also calculated. The standard deviation measures the amount of variation or dispersion from the average. A low standard deviation indicates that the data points tend to be very close to the expected value (mean); a high standard deviation indicates that the data points are spread out over a large range of values. The expression to calculate this variable is:

$$s_N = \sqrt{\frac{1}{N} \sum_{i=1}^{N} (x_i - \bar{x})^2} \qquad \text{(Eq. 4.2)}$$

4.3. Frequency-domain analysis

A feature, which theoretically should be useful for the purpose of sedation analysis, is the change of the spectral properties of the EEG activities during a surgical operation. The frequency-domain analysis was calculated by using the Power Spectral Density (PSD).

An EEG contains a wide range of frequency components. However, the range of clinical and physiological interests is between 0.1 and 45 Hz. The rhythms of the EEG are classified into six main groups depending on the predominant frequency contents: Delta rhythm (0.1-4 Hz), Theta rhythm (4-8 Hz), Alpha rhythm (8-12 Hz), Beta rhythm (12-30 Hz), total frequency (TB) rhythm (0.1-45 Hz) and ALL spectrum (ALL) (0-45 Hz).

For each passage the power spectral densities were estimated using a 50th FIR filter for the bands: Delta, Theta, Alpha, Beta and TB. Moreover, for each respective band the following variables were defined: $PSD_\delta, PSD_\theta, PSD_\alpha, PSD_\beta, PSD_{TB}$. After a statistical analysis was applied to this proposed set of variables to find characteristic patterns and information for each EEG band.

In this thesis the *PSD* value has been normalized estimating the total area under the *PSD* curve. Consequently, the *PSD* always has a unitary value and for this reason it has not been proposed as a variable for this study.

4.4. Non-linear dynamic analysis

4.4.1. Symbolic Dynamics

The non-linear EEG dynamics were analyzed by means of symbolic dynamics. Each EEG segment was transformed into symbols, in order to preserve the essential and robust properties of the dynamics present in the EEG signals. There are diverse ways of coding the EEG signals, that is to say, you can translate data into several given alphabets.

4.4.2. Equidistant analysis

The symbolic dynamics method based on [39] was applied to the GAG signal. This series was uniformly spread on 6 levels. First, it was calculated the distance between minimum and maximum value for each signal. After that, the distance was divided by the number of levels (n=6) and each level (see Eq. 4.3) was determined by the equation:

$$L_i = L_{i-1} + \frac{max - min}{n} \qquad \text{(Eq. 4.3)}$$

From the symbol string L_i, M=216 word types $ijk = \{111, 112, 113, \ldots, 664, 665, 666\}$ consisting of three successive symbols with an overlap of 2 symbols were defined. The word probability of occurrence is defined as w_{ijk} and the level probability of occurrence is defined as l_i. The l_i is the probability of occurrence of each individual symbol.
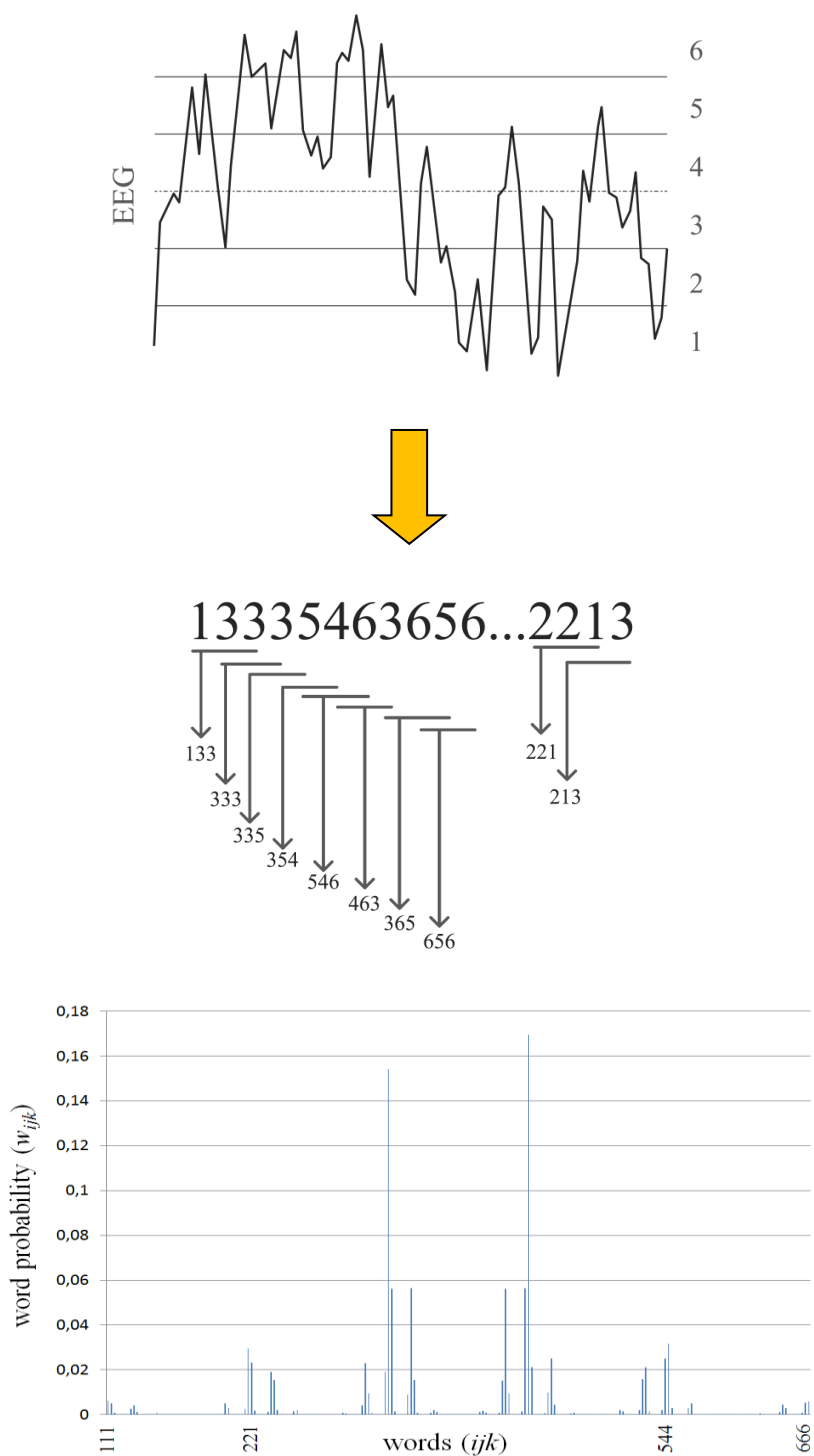
Fig. 4.3. Symbolic dynamics methodology. The signal is transformed into a symbols series using an EQ algorithm. The words ijk are constructed and the probabilities w_{ijk} are evaluated.

4.4.3. Non-equidistant analysis

The non-linear EEG dynamics were also analyzed by the [40] symbolic dynamic method. Each EEG segment is transformed into four symbol sequences with symbols from a given alphabet {0,1,2,3}. Some detailed information is lost in the process but the coarse dynamic behavior can be analyzed. The following equation indicates the signal transformation into four non-equidistant levels, where $EEG_m(i)$ is the $EEG(i)$ series after adding the mean value of its amplitude range.

$$S_i = \begin{cases} 0: & \overline{EEG_m} \leq EEG_m(i) < (1+a)\overline{EEG_m} \\ 1: & (1+a)\overline{EEG_m} \leq EEG_m(i) < \infty \\ 2: & (1-a)\overline{EEG_m} \leq EEG_m(i) < \overline{EEG_m} \\ 3: & 0 \leq EEG_m(i) < (1-a)\overline{EEG_m} \end{cases}$$

Where $\overline{EEG_m}$ is the mean value of $EEG_m(i)$.

Then, a new series S_i was obtained for each EEG segment, where i=1, 2, 3,…, N samples. The parameter a was set to {0.01, 0.025, 0.05, 0.0625, 0.075, 0.0875, 0.1, 0.125} in order to match the standard deviation of the $EEG(i)$ series. From the symbol string S_i, M=64 word types $ijk = \{000, 001, 002, \ldots, 331, 332, 333\}$ consisting of three successive symbols with an overlap of 2 symbols were defined.
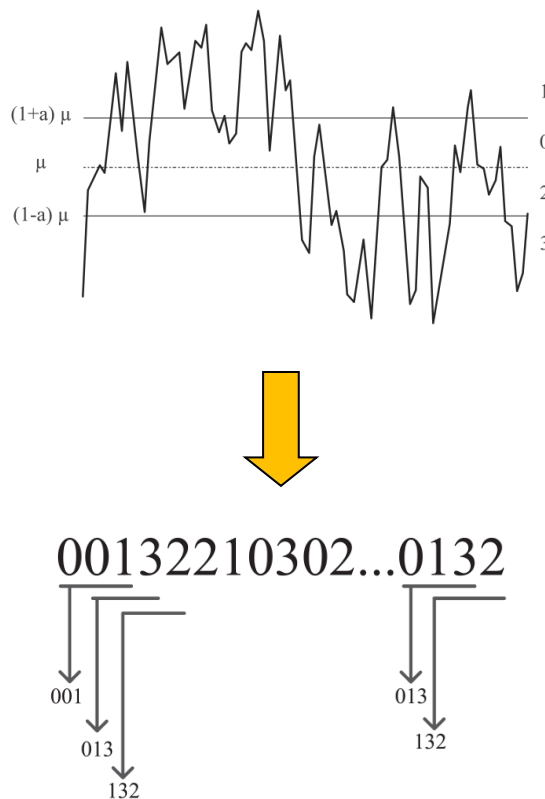
Fig. 4.4. Symbolic dynamics methodology using a NEQ algorithm.

4.4.4. Construction of variables

Six types of variables based on the distribution of words ijk were estimated. The first four variables were calculated using the alphabet explained in the previous subsection.

- w_{ijk}, occurrence probability of each one of the word types (Fig. 4.5).
- l_i, occurrence probability of the symbols at each level.
- $fw(THf)$, number of forbidden words whose probability of occurrence w_{ijk} is lower than a probability threshold $THf = \{0.01, 0.005, 0.001, 0.0005\}$.
- $pw(THp)$, number of words whose probability of occurrence $P(w_{ijk})$ is higher than a probability threshold $THp = \{0.025, 0.05, 0.1, 0.2, 0.3, 0.5\}$.
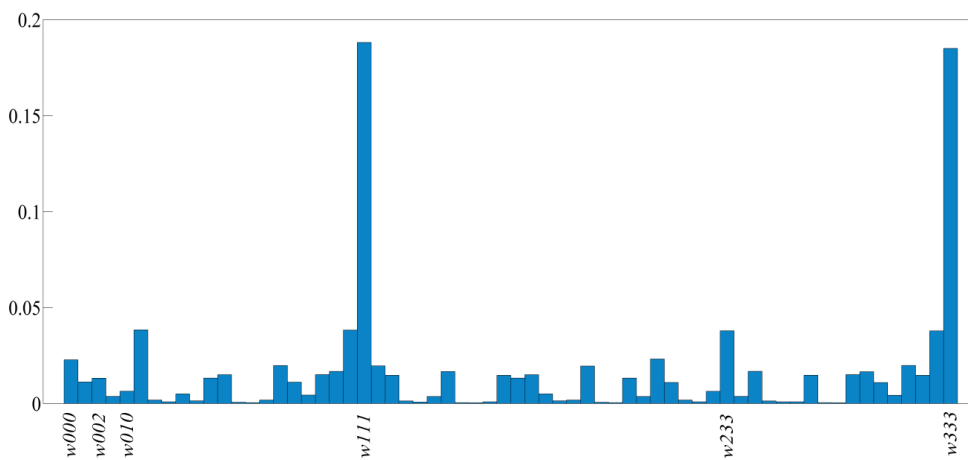
Fig. 4.5. Example of the probability of occurrence of the words variables (w_{ijk}) measured for one patient (RSS={6}, a=0.1, Total Band).

Then, patterns of length *L*=3 consecutive symbols with an overlapping of two symbols were constructed. All possible patterns were grouped into 3 families referred to as: $v0$, patterns with no variation (all 3 symbols were equal); $v1$, patterns with one variation (2 consequent symbols were equal and the remaining symbol was different); $v2$, patterns with 2 variations (all symbols were different from the previous one).

For each family, different kinds of variations, named subfamilies, were defined as it can be seen in Fig. 4.6. In the case of *v0*, one pattern can have all values higher than the third level ($v0_u$, 0 variation, up) or lower than the third level $v0_d$, 1 variation, down). In *v1* case, there are 4 different kinds of variations: $v1_{eu}, v1_{ue}, v1_{de}, v1_{ed}$, where e means equal (i.e., two consequent symbols are in the same level), u is for up (i.e., next symbol is in a level higher than the previous one), and d means down (i.e., next beat is in a lower level than the previous one). Finally, pattern *v2* is characterized by 4 variants: $v2_{du}, v2_{ud}, v2_{dd}, v2_{uu}$.
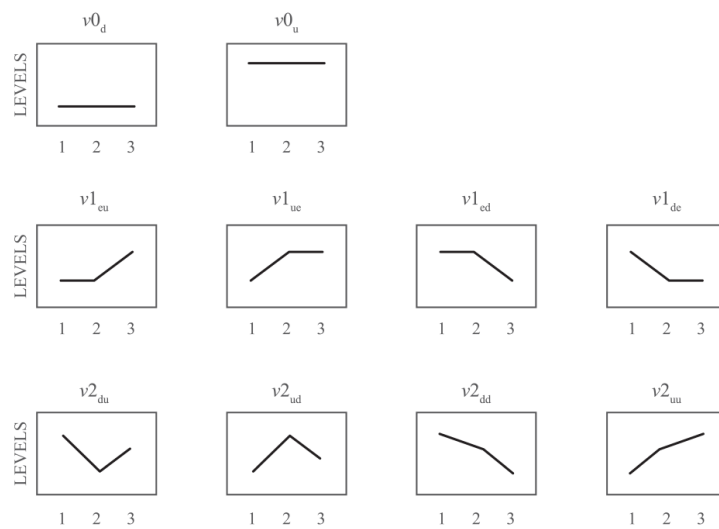
Fig. 4.6. Classification of the variability patterns.

Finally, two more types of variables were estimated making use of the patterns explained above:

- F_m, occurrence probability (see Fig. 4.7) of each of the three family patterns $F_m = \{v0, v1, v2\}$ (m=1,…,3) where M=3 type of patterns.

- sF_m, occurrence probability of each of the ten subfamily patterns $sF_m = \{v0_u, v0_d, v1_{eu}, v1_{ue}, v1_{de}, v1_{ed}, v2_{du}, v2_{ud}, v2_{dd}, v2_{uu}\}$ (m=1,..,10) where M=10 type of patterns (see Fig. 4.8).
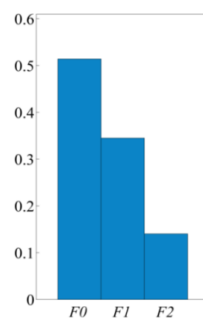
Fig. 4.7. Example of the probability of occurrence of the Families (F_m) variables measured for one patient (RSS={6}, a=0.1, Total Band).
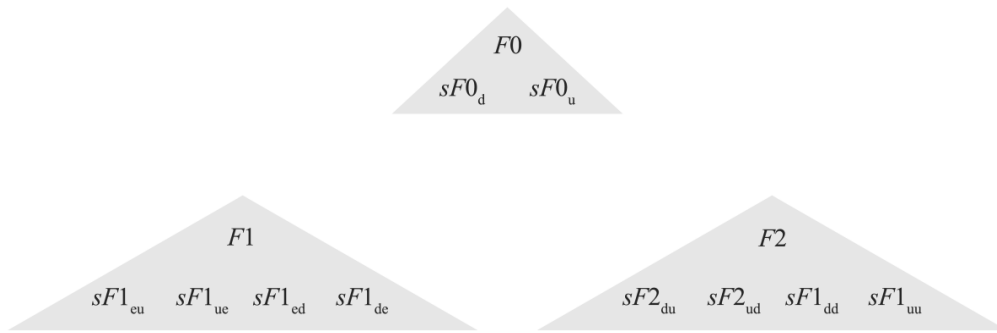
Fig. 4.8. Classification in Families and Subfamilies patterns.

4.4.5. Shannon and Rényi entropy

Also, Shannon entropy (SH) and Rényi entropy (Hq) (Eq. 4.4 and Eq. 4.5), which are the classic measures for the complexity in time series, were calculated from the distribution of patterns of $F0$, $F1$ and $F2$ (z=1,..,3).

$$SH = - \sum_{m=1}^{M} P_m \, log_2(P_m) \qquad (Eq.\,4.4)$$

P_m is used as general notation to represent the four variables used to estimate the Shannon entropy: w_{ijk}, l_i, F_m and sF_m.

SH_w represents the Shannon entropy calculated for a w_{ijk} variable.

SH_l represents the Shannon entropy calculated for a l_i variable.

SH_F represents the Shannon entropy calculated for a F_m variable.

SH_{SF} represents the Shannon entropy calculated for a sF_m variable.

In this study, Rényi entropy (Eq. 4.5) was estimated for different values of q parameter q = {0.1, 0.2, 0.3, 0.4, 0.5, 0.6, 0.7, 0.8, 0.9, 1.5, 2, 2.5, 3}.

$$H_q = \frac{1}{q-1} log_2 \left(\sum_{m=1}^{M} P_m^q \right) \qquad (Eq.\,4.5)$$

P_m is used as general notation to represent the four variables used to estimate the Rényi entropy: w_{ijk}, l_i, F_m and sF_m.

Hqw represents the Rényi entropy calculated for a w_{ijk} variable.

Hql represents the Rényi entropy calculated for a l_i variable.

HqF represents the Rényi entropy calculated for a F_m variable.

$HqsF$ represents the Rényi entropy calculated for a sF_m variable.

Large probabilities dominantly influence the Rényi entropy if $q > 1$ and small probabilities mainly determine the value of this entropy if $0 < q < 1$ (Eq. 4.5). When q tends to unity, Rényi entropy converges to Shannon entropy.

4.5. Statistical analysis

The aim of the statistical analysis is to evidence variables able to discriminate between the different zones and to observe how the selected variables classify an unknown series of data in the correct zone during the validation process.

The statistical analysis has been carried out using MATLAB and SPSS (Statistical Package for the Social Sciences). SPSS is a computer application that provides statistical analysis of data. It allows in-depth data access and preparation, analytical reporting, plotting and modeling.

The statistics used in the present work are:

- Bivariate statistics: basic statistics (means, standard deviations, etc.), non-parametric tests (Mann-Whitney), Spearman's correlation.
- Prediction for identifying groups: Discriminant function
- Validation for identifying groups: Leaving-one-out method.

This part presents the nomenclature chosen to name the variables in order to classify the data in groups. The RSS and the GAG states are the characteristic information that provides help to separate each EEG passage and find the differences. Every trial study includes two groups depending on the responsive state:

- GAG corresponds to GAG analysis.
- trial 1 studies the responsive state RSS={2,3,4,5} versus RSS={6}.
- trial 2 studies the responsive state RSS={3,4,5} versus RSS={6}.
- trial 3 studies the responsive state RSS={4,5} versus RSS={6}.
- trial 4 studies the responsive state RSS={5} versus RSS={6}.

4.5.1. Measuring linear association: Spearman's correlation

Spearman's rank correlation coefficient is a nonparametric (distribution-free) rank statistic proposed by Charles Spearman as a measure of the strength of an association between two variables. It is a measure of a monotone association that is used when the distribution of data makes Pearson's correlation coefficient undesirable or misleading. Spearman's coefficient is not a measure of the linear relationship between two variables. It assesses how well an arbitrary monotonic function can describe a relationship between two variables, without making any assumptions about the frequency distribution of the variables. Unlike Pearson's product-moment correlation coefficient, it does not require the assumption that the relationship between the variables is linear, nor does it require the variables to be measured on interval scales; it can be used for variables measured at the ordinal level. Spearman's correlation is the measure chosen in this thesis.

To understand Spearman's correlation it is necessary to know what a monotone function is. A monotone function is one that either never increases or never decreases as its independent variable increases. The following Fig. 4.9 illustrates monotone functions:
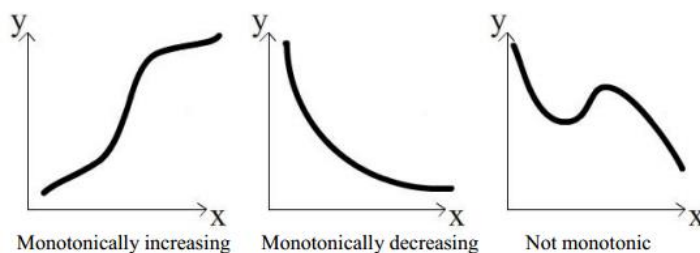
Fig. 4.9. Different examples of monotone functions.

Spearman's correlation is usually referred as r_s. The r_s gives a value between +1 and −1 inclusive, where 1 is total positive correlation, 0 is no correlation, and −1 is total negative correlation.

The Spearman correlation coefficient (see Eq. 4.6) is defined as the Pearson correlation coefficient between the ranked variables. For a sample of size n, the n raw scores X_i, Y_i are converted to ranks x_i, y_i, and r_s is computed from:

$$r_s = 1 - \frac{6 \sum d_i^2}{n(n^2 - 1)} \qquad (Eq. 4.6)$$

where $d_i = x_i - y_i$, is the difference between ranks.

The formula for correlation is useful to see that r_s is positive when there is a positive association between the ranks. A more detailed study of the formula gives more detailed properties of r_s. The

following is a list of important things to know in order to interpret correlation and understand how it should be used.

1. An advantage with this measure is that it is much easier to use since it does not matter which way the data is ranked, ascending or descending. The rank may be assigned 1 to the smallest value or the largest value, provided the same thing for both sets of data is done.
2. Positive r_s indicates positive association between the ranks, and negative r_s indicates negative association.
3. The correlation r_s is always a number between -1 and 1. Values of r_s near 0 indicate a very weak monotone relationship. The strength of the monotone relationship increases as r_s moves away from 0 toward either -1 or 1. The extreme values $r_s = -1$ and $r_s = 1$ occur only in the case when each of the variables is a perfect monotone function of the other.

Moreover, its interpretation is similar to that of Pearson's, e.g. the closer is to 1 the stronger the monotone relationship. Correlation is an effect size and so we can verbally describe the strength of the correlation using the following guide for the absolute value of:

- 0.00-.19 "very weak"
- 0.20-.39 "weak"
- 0.40-.59 "moderate"
- 0.60-.79 "strong"
- 0.80-1.0 "very strong"

The calculation of Spearman's correlation coefficient and subsequent significance testing of it requires the following data assumptions to hold:

- The two variables should be measured on an ordinal, interval or ratio scale (continuous).
- There needs to be a monotonic relationship between the two variables.

Note, unlike Pearson's correlation, there is no requirement of normality and hence it is a nonparametric statistic.

4.5.2. Non-parametric tests

The most commonly used methods for inference about the means of quantitative response variables assume that the variables in question have Normal distributions in the population from which data is drawn. In practice, no distribution is exactly Normal. Fortunately, usual methods for inference about population means (the one-sample and two-sample t procedures and analysis of variance) are quite robust. That is, the results of inference are not very sensitive to moderate lack of Normality, especially when the samples are reasonably large.

ETSEIB

After applying one-sample Kolmogorov-Smirnov test to the EEG, the test rejected the null hypothesis that the data analyzed comes from a standard normal distribution. For that reason, parametric statistical methods cannot be used to test statistical significance of the data. That is to say, any specific form for the distribution can be assumed. Unlike bootstrap and permutation methods, common non-parametric methods do not make use of the actual values of the observations.

The following subsection concerns one type of non-parametric procedure: tests that can replace the t tests and one-way analysis of variance when the Normality conditions for those tests are not met. The most useful non-parametric tests are rank tests based on the rank (place in order) of each observation in the set of all the data.

Table 4.1 presents an outline of the standard tests (based on Normal distributions) and the rank tests that compete with them. The rank tests require that the population or populations have continuous distributions. That is, each distribution must be described by density curve that allows observations to take any value in some interval of outcomes. The Normal curves are one shape of density curve.

Setting	Normal test	Rank test
One sample	One-sample t test	Wilcoxon signed rank test
Matched pairs	Apply one-sample test to differences within pairs	
Two independent samples	Two-sample t test	Wilcoxon rank sum test
Several independent samples	One-way ANOVA F test	Kruskal-Wallis test

Table 4.1. Tests used to verify statistical hypothesis depending on the data type.

In this thesis, to compare the differences between two independent samples it will be applied the Wilcoxon rank sum test which is explained below. In this next setting, it will also be explained ideas common to all rank test.

4.5.3. Wilcoxon rank sum test

The Wilcoxon test is a non-parametric test [41] based upon ranking the total number of observations of the combined sample. The test sums the ranks for observations from one of the samples and uses the ranks to assess whether two independent samples belong to distributions with equal medians, against the alternative that the distribution does not have identical medians. The test is equivalent to Mann-Whitney U-test. The hypotheses for the comparison of two independent groups are:

H_0: The two samples came from identical populations ($\mu_1 = \mu_2$).

H_a: The two samples came from different populations ($\mu_1 \neq \mu_2$).

The statistic test for the Wilcoxon test is the rank sum W. To make the statistical test calculation, all samples are combined and ordered form the smallest to the highest value. The number of the ranking is associated to each sample and, considering which class they belong to, the W is calculated as the sum of the rank of the samples that come from the same group. The obtained value W is used in a set of Tables in order to decide if the null hypothesis is accepted or rejected. The tables contain critical values for significant levels as different probabilities to reject the H_o, against the group size. The critical value has to be compared to the rank sum value W and the result of the test is collected. For example, if W is lower than the critical value for the significance level 0.05, it means that there is a probability of 5% to reject the H_o when this hypothesis is true and the difference between the two groups was unlikely to occur by chance. Otherwise, there is evidence to reject the null hypothesis H_o in favor of the alternative hypothesis H_a.

The statistic test for the Mann-Whitney test is U. As in the Wilcoxon test, all samples are combined and ordered before evaluate the U. The following Eq. 4.7 is used for the definition of the U test.

$$U = min \begin{cases} U_1 = R_1 - \dfrac{n_1(n_1 + 1)}{2} \\ U_2 = R_2 - \dfrac{n_2(n_2 + 1)}{2} \end{cases} \quad \text{(Eq. 4.7)}$$

Where n_1 and n_2 are the number of the samples of each class, and R_1 and R_2 are the sum of the ranks of each class. This value is compared to a table of critical value for U based on the sample size of each group. If U exceeds the critical value for U at some significance level (usually 0.05) it means that there is evidence to reject the null hypothesis H_o in favor of the alternative hypothesis H_a. If this value exceeds the critical value for U at the significance level 0.05, it means that there is a probability of 5% to reject H_o when the hypothesis is true.

In this study, the variables with $p - value < 0.05$ are considered able to distinguish the groups and highlight differences.

4.5.4. Bonferroni correction

In statistics, the Bonferroni correction is a method used to address the problem of multiple comparisons. Null hypothesis is rejected for rare events, and the larger is the number of tests, the easier is to find rare events which are false alarm (H_0 is rejected when it is true, *Type 1 error*). This problem is called inflation of the confidence level. In order to avoid this error, one strategy is to correct the significance level when performing multiple tests. Marking the level more stringent (i.e., smaller) will create less errors, but it may also make it harder to detect real effects.

ETSEIB

The correction is based on the idea that if an experiment is testing m dependent or independent hypothesis on a set of data, a way of ensuring the error rate as if only one hypothesis was tested, is to rest each distinct hypothesis at a statistical level of $1/m$ times. Thus, if the significance level for the whole family of tests is required to be (at most) α, applying the Bonferroni correction, each test will be conducted with a confidence level of $\frac{\alpha}{m}$.

In this work, because of the large number of symbolic dynamics tests, Bonferroni correction is applied to the proposed variables.

$$significant\ level\ of\ N_\alpha = \frac{\alpha}{W} = \frac{0.05}{7265} = 6.88E - 06$$

4.5.5. Discriminant function

The aim is to find a tool that allows to discriminate between groups (states) so that, when there is a new series (EEG segment) and it is unknown its belonging group, the method tries to find the best correctly classification. There are many possible techniques for classification of data. Linear discriminant analysis (LDA) is a commonly used technique for data classification and dimensionality reduction. The objective of linear discriminant analysis is to perform dimensionality reduction while preserving as much of the class discriminatory information as possible. The linear discriminant analysis can be divided into two different approaches:

Class-dependent. This type of approach involves maximizing the ratio of between class variance to within class variance. The main objective is to maximize this ratio in order to obtain an adequate class separation.

Class-independent. This approach involves maximizing the ratio of overall variance to within class variance. In this type of LDA, each class is considered as a separate class against all other classes.

The method applied in this work is the class-dependent approach, seeking to find directions along which the classes are best separated by maximizing the ratio of the between-class variance to the within class (Balakrishnama *et al.*, 1998).

In this work, the linear discriminant analysis for data classification is applied to classification problem in DOA. In particular, the aim of the LDA is to evaluate the discriminant power of variables between two different zones. For this purpose, discriminant classification functions are shaped on the variables previously obtained in time and frequency domain and also obtained with symbolic dynamics, the application of thresholds and evaluation of entropies.

A classification function was defined for each variable analysis, coupling them from two different groups. The groups evaluated in this work with LDA are four RSS groups and two GAG groups. The discriminant analysis is a linear combination of independent variables which served as a basis for

assigning cases to each group. Thus the information contained in multiple independent variables is summarized in an index, which will be used to make the separation between groups. The Eq. 4.8 of the discriminant function is:

$$S_i = w_{i0} + w_{i1}x_1 + w_{i2}x_2 + \cdots + w_{im}x_m \qquad (Eq. 4.8)$$

where, the subscript i denotes the respective class; the subscripts 1, 2, ..., m denote the number m of variables; w_{i0} is a constant for the *i-th* class, w_{ij} is the weight for the *j-th* variable in the computation of the classification score for the *i-th* class; x_j is the observed value for the respective *j-th* variable. The resultant classification score is S_i. As it can be noticed the equation of the discriminant function is very similar to multiple linear regressions.

The first step for classification is to build a discriminant function by estimating the coefficients w_{jm}: the purpose is making S_j different as much as possible between the groups. The rate used is the one that maximizes the between-class scatter while minimizing the within-class scatter. Let μ_j be the mean vector of the *j-th* group, let m be the number of variables within the group j, the within-class scatter matrix S_w (see Eq. 4.9) and the between-class scatter matrix S_b (see Eq. 4.10) are respectively:

$$S_w = \sum_{j=1}^{2}\sum_{i=1}^{m}(x_i - \mu_j)(x_i - \mu_j)^T \qquad (Eq. 4.9)$$

$$S_b = \sum_{j=1}^{2}(\mu_j - \mu)(\mu_j - \mu)^T \qquad (Eq. 4.10)$$

Where the mean (Eq. 4.11) on the entire data set is:

$$\mu_s = \frac{1}{2}\sum_{j=1}^{2}\mu \qquad (Eq. 4.11)$$

The coefficient of the discriminant functions (Fig. 4.10) are the values that maximize (Eq. 4.12) the ratio between of S_b and S_w, as in the following expression:

$$\max\left(\frac{det(S_b)}{det(S_w)}\right) \qquad (Eq. 4.12)$$

After obtaining the coefficients, values of S_i are calculated substituting the variable value m in x_m of (Eq. 4.8) for each *i*-case. For each S_i value a case is classified comparing its value with a threshold value of each class (generally $S_{th} = 0$).
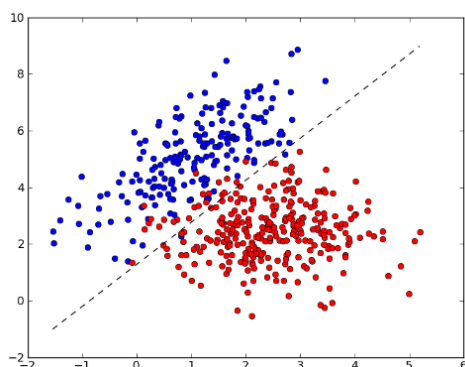
Fig. 4.10. Example of application of linear discriminant analysis (LDA). The goal of the LDA is to find the best linear function that permits to separate the two sets of data.

4.5.6. Estimation of the proportion of bad classified cases

One model usually classifies in the best possible way exactly the population that has been used to develop it than any other. Therefore, if the discriminant function is applied on the cases that have helped build it, the proportion of bad classified cases will estimate how much that differ from the true.

There are many ways to obtain the best estimate of the proportion of cases not correctly classified. If the sample is sufficiently long to be divided into two parts, one can be used to find the discriminant function and the other to test it. As the cases themselves will not be used to estimate and validate the function, the error rate observed in the sample 'test' would better reflect the effectiveness of discriminant function.

In the present work, the same database has been used for the validation, which has been carried on simultaneously to the classification as we used the leave-one-out method.

4.5.7. Cross Validation: leaving-one-out method

Cross-validation is a technique for assessing how the results of a statistical analysis will generalize to an independent data set (Geisser, 1993; Kohavi, 1995; Devijver, 1982). It is mainly used in settings where the goal is prediction, and one wants to estimate how accurately a predictive model will perform in practice.

One round of cross-validation involves partitioning a sample of data into complementary subsets, performing the analysis on one subset (the training set), and validating the analysis on the other subset (the validation set). To reduce variability, multiple rounds of cross-validation are performed using different partitions, and the validation results are averaged over the rounds.

Cross-validation is a generally applicable way to predict the performance of a model on a validation set using computation in place of mathematical analysis. As the name suggests, leave-one-out cross-validation (LOOCV) involves using a single observation from the original sample as the validation data, and the remaining observations as the training data. This is repeated such that each observation in the sample is used once as the validation data. Leave-one-out cross-validation is usually very expensive from a computational point of view because of the large number of times the training process is repeated. If a validation test, different from the training set, is not available, any type of validation similar to this is the most reliable.

4.5.8. Specificity, sensibility and accuracy

Specificity (Eq. 4.13) measures the proportion of negatives which are correctly identified. To perform the calculation it will be used the following equation:

$$Specificity(\%) = \frac{VP}{VP + FN} * 100 \qquad (Eq. 4.13)$$

Where VP are the subjects identified correctly in the class that we are analyzing, while FN are the ones identified as belonging to the other class.

The sensitivity (Eq. 4.14) measures the proportion of actual positives which are correctly identified as such:

$$Sensibility(\%) = \frac{VN}{VN + FN} * 100 \qquad (Eq. 4.14)$$

Where VN are the subjects identified correctly as not belonging to the class that we are analyzing, while FP are the ones identified wrongly as belonging to this class.

A theoretical, optimal prediction can achieve 100% sensitivity and 100% specificity. The diagnostic accuracy (Eq. 4.15), a more general parameter, is defined as the proportion of individuals correctly classified.

$$Diagonistic\ Accuracy(\%) = \frac{VP + VN}{VP + VN + FP + FN} * 100 \qquad (Eq. 4.15)$$

4.5.9. Definition and interpretation of P_k

Ideally, anesthetic depth indicator value should correlate perfectly with anesthetic depth along a lighter-deeper anesthesia continuum. Experimentally, however, an anesthetic depth indicator is judged against a "gold standard" indicator that provides only quantal observations of anesthetic depth. The standard anesthetic depth indicator is the patient's response to specific stimuli.

ETSEIB

The ability of the parameters to describe loss of consciousness and anesthetic depth is evaluated using prediction probability (P_k), which compares the performance of indicators having different units of measurements, as developed by Smith and colleagues. P_k is calculated using Somer's d-test with linear transformation to the range of 0– 1, where 1 corresponds to an exact prediction of the clinical scale, whereas 0.5 is not better than tossing a fair coin. In this way the P_k is a performance which shows the correlation between anesthetic depth indicator value and observed anesthetic depth, taking into account both desired performance and the limitations of the data. Prediction probability has a value of 1 when the indicator predicts observed anesthetic depth perfectly and a value of 0.5 when the indicator predicts no better than a 50:50 chance. Prediction probability avoids the shortcomings of other measures. For example, as a nonparametric measure, P_k is independent of scale units and does not require knowledge of underlying distributions or efforts to linearize or to otherwise transform scales.

Furthermore, P_k can be computed for any degree of coarseness or fineness of the scales for anesthetic depth indicator value and observed anesthetic depth; thus, P_k fully uses the available data without imposing additional arbitrary constraints. Finally, P_k can be used to conduct both grouped and paired-data statistical comparisons of anesthetic depth indicator performance.

Prediction probability P_k is a variant of Kim's measure of association. Kim's $d_{x \cdot y}$ (Eq. 4.16) is defined for ordinal variables x and y in terms of the types of pairs of data points just described. Let P_c, P_d, and P_{tx} be the respective probabilities that two data points drawn at random, independently and with replacement, from the population are a concordance, a discordance, or an x-only tie. The only other possibility is that the two data points are tied in observed depth y; therefore, the sum of the three kinds of probability is the probability that the two data points have distinct values of observed anesthetic depth, that is, that they are not tied in y.

Kim's $d_{x \cdot y}$ is defined by:

$$d_{x \cdot y} = \frac{P_c}{P_c + P_d + P_{tx}} - \frac{P_d}{P_c + P_d + P_{tx}} = \frac{P_c - P_d}{P_c + P_d + P_{tx}} \qquad (Eq. 4.16)$$

Alternatively, prediction probability P_k (Eq. 4.17) defiend as:

$$P_k = \left(d_{x \cdot y} + 1 \right) \qquad (Eq. 4.17)$$

Which, by inserting Eq. 4.16 into Eq. 4.17, becomes Eq. 4.18:

$$P_k = \frac{P_c + \frac{1}{2} P_{tx}}{P_c + P_d + P_{tx}} \qquad (Eq. 4.18)$$

Thus, P_k and Kim's $d_{x \cdot y}$ differ in scale and range of values but convey the same information. As desired, both Kim's $d_{x \cdot y}$ and P_k reward concordances, penalize discordances and indicator-only ties,

and ignore ties in observed depth y. The range for Kim's $d_{x \cdot y}$ is from -1 to +1, while that for P_k is from 0 to 1. When the probabilities of discordance and indicator-only tie are both zero then $d_{x \cdot y}$ and P_k both equal 1. When the probability of discordance equals that of concordance, $d_{x \cdot y} = 0$ and $P_k = 0.5$. If $d_{x \cdot y} < 0$ or $P_k < 0.5$ the discordances are more likely than concordances.

A performance measure for assessing proposed anesthetic depth indicators must be selected with care to avoid false conclusions about the potential utility of an indicator or how it compares with other indicators. The measure should have a meaningful interpretation and permit statistical comparisons of performance. More specifically, the measure should take into account the relationship desired between anesthetic depth indicator value and anesthetic depth and the nature of the available experimental data. In doing so, it should not require unjustified assumptions or ignore available information in the data.

Chapter 5

Results and discussion

The present chapter contains the results of the applied methodology based on time-domain, frequency-domain and symbolic dynamics variables. Also, the statistical analysis of the variables is presented.

5.1. Time-domain and frequency-domain analysis

An analysis of the dataset in time and frequency domain was conducted for each passage collected. The variables studied in this subsection are listed below:

- The A-Line Arx index (AAI).
- Bispectral Index (BIS).
- Ce_{propo}
- Ce_{remi}
- Standard Deviation (SD).
- Power Spectral Density of the Delta band (PSD_δ).
- Power Spectral Density of the Theta band (PSD_θ).
- Power Spectral Density of the Alpha band (PSD_α).
- Power Spectral Density of the Beta band (PSD_β).
- Power Spectral Density of the Total band (PSD_{TB}).

Tables 5.1 to 5.4 contain the performance obtained from the statistical analysis of the clinical variables: AAI, BIS, Ce_{propo} and Ce_{remi}. In Table 5.5, the results of the SD are presented. Finally, Tables 5.6 to 5.10 show the results of the Power Spectral analysis. The best P_k values, $0.6 < P_k \le 0.76$, corresponding to Trial 4 and GAG were obtained by AAI, BIS, Ce_{remi}, SD. The values of AAI and BIS for each group follow the proper scale of the sedation level. The values of Ce_{propo} and Ce_{remi} increase with the level of sedation and analgesia, respectively. Standard deviation, SD, was also able to differentiate groups {5}vs{6} in RSS due to the ASEF filter [38] with P_k =0.648. The values of PSD in all the frequency bands increase from group RSS= {2,3,4,5} to RSS= {6}.

AAI	Groups	mean ± sd	Statistics	p-value	P_k
RSS	{2,3,4,5}	34.2 ± 19.2	Trial 1 {2,3,4,5}vs{6}	6.43E-18	0.802
	{3,4,5}	30.6 ± 17. 7	Trial 2 {3,4,5}vs{6}	3.57E-132	0.767
	{4,5}	24.0 ± 13.8	Trial 3 {4,5}vs{6}	7.71E-96	0.698
	{5}	22.3 ± 12.1	Trial 4 {5}vs{6}	5.99E-42	0.648
	{6}	18.2 ± 9.9			
GAG	{0}	25.8 ± 16.6	GAG {0} vs {1}	6.43E-18	0.755
	{1}	40.7 ± 19.1			

Table 5.1. Clinical analysis results of the AAI variable.

BIS	Groups	mean ± sd	Statistics	p-value	P_k
RSS	{2,3,4,5}	76.6 ± 13.7	Trial 1 {2,3,4,5}vs{6}	4.61E-130	0.799
	{3,4,5}	73.87 ± 13.1	Trial 2 {3,4,5}vs{6}	1.35E-93	0.764
	{4,5}	69.3 ± 12.9	Trial 3 {4,5}vs{6}	2.25E-38	0.689
	{5}	65.7 ± 13.7	Trial 4 {5}vs{6}	3.06E-11	0.622
	{6}	59.9 ± 14.3			
GAG	{0}	68.3 ± 15.0	GAG {0} vs {1}	1.37E-15	0.738
	{1}	80.5 ± 11.9			

Table 5.2. Clinical analysis results of the BIS variable.

Ce_{propo}	Groups	mean ± sd	Statistics	p-value	P_k
RSS	{2,3,4,5}	1.83 ± 0.907	Trial 1 {2,3,4,5}vs{6}	1.56E-55	0.693
	{3,4,5}	2.04 ± 0.787	Trial 2 {3,4,5}vs{6}	1.97E-27	0.639
	{4,5}	2.22 ± 0.738	Trial 3 {4,5}vs{6}	1.18E-6	0.571
	{5}	2.36 ± 0.705	Trial 4 {5}vs{6}	$0.910^{n.s.}$	0.502
	{6}	2.38 ± 0.669			
GAG	{0}	2.42 ± 0.718	GAG {0} vs {1}	8.67E-2	0.550
	{1}	2.31 ± 0.780	*n.s. statistically non-significant level*		

Table 5.3. Clinical analysis results of the C_{propo} variable.

Ce_{remi}	Groups	mean ± sd	Statistics	p-value	P_k
RSS	{2,3,4,5}	1.1 ± 0.815	Trial 1 {2,3,4,5}vs{6}	3.30E-23	0.622
	{3,4,5}	1.15 ± 0.793	Trial 2 {3,4,5}vs{6}	1.67E-16	0.606
	{4,5}	1.15 ± 0.805	Trial 3 {4,5}vs{6}	7.03E-12	0.600
	{5}	1.03 ± 0.820	Trial 4 {5}vs{6}	9.98E-15	0.642
	{6}	1.39 ± 0.598			
GAG	{0}	1.40 ± 0.646	GAG {0} vs {1}	2.35E-5	0.625
	{1}	1.15 ± 0.811			

Table 5.4. Clinical analysis results of the C_{remi} variable.

ETSEIB

SD	Groups	mean ± sd	Statistics	p-value	P_k
RSS	{2,3,4,5}	1442.1 ± 605.2	Trial 1 {2,3,4,5}vs{6}	2.204E-17	0.802
	{3,4,5}	1381.0 ± 531.3	Trial 2 {3,4,5}vs{6}	5.684E-11	0.767
	{4,5}	1380.7 ± 532.7	Trial 3 {4,5}vs{6}	8.527E-9	0.698
	{5}	1426.7 ± 528.8	Trial 4 {5}vs{6}	6.258E-10	0.648
	{6}	1249.3 ± 544.2			
GAG	{0}	1398.7 ± 660.6	GAG {0} vs {1}	0.0969$^{n.s.}$	
	{1}	1548.2 ± 834.4	*n.s. statistically non-significant level*		

Table 5.5. Time-domain analysis results of the SD variable.

Tables 5.6 to 5.10 contain the frequency-domain analysis results. The *PSD* in the frequency bands δ, θ and α was able to differentiate the RSS groups of trial 4 with a $0.6 < P_k \leq 0.65$. Analyzing the groups of GAG, the *PSD* was able to discriminate the group in the δ, θ, α, β and *TB* bands with a $0.6 < Pk \leq 0.75$. The values of *PSD* increase towards to the least responsive level, RSS={6} and GAG={0}.

PSD_δ	Groups	mean ± sd	Statistics	p-value	P_k
RSS	{2,3,4,5}	0.094 ± 0.011	Trial 1 {2,3,4,5}vs{6}	1.28E-53	0.690
	{3,4,5}	0.094 ± 0.010	Trial 2 {3,4,5}vs{6}	1.06E-49	0.690
	{4,5}	0.096 ± 0.010	Trial 3 {4,5}vs{6}	4.40E-25	0.651
	{5}	0.098 ± 0.009	Trial 4 {5}vs{6}	1.28E-10	0.618
	{6}	0.101 ± 0.009			
GAG	{0}	0.096 ± 0.010	GAG {0} vs {1}	3.98E-4	0.605
	{1}	0.092 ± 0.011			

Table 5.6. Frequency-domain analysis results of the PSD_δ variable.

PSD_θ	Groups	mean ± sd	Statistics	p-value	P_k
RSS	{2,3,4,5}	0.094 ± 0.011	Trial 1 {2,3,4,5}vs{6}	9.63E-101	0.762
	{3,4,5}	0.096 ± 0.011	Trial 2 {3,4,5}vs{6}	4.66E-75	0.735
	{4,5}	0.099 ± 0.010	Trial 3 {4,5}vs{6}	5.59E-30	0.666
	{5}	0.101 ± 0.009	Trial 4 {5}vs{6}	6.93E-11	0.620
	{6}	0.104 ± 0.009			
GAG	{0}	0.098 ± 0.012	GAG {0} vs {1}	1.93E-12	0.708
	{1}	0.089 ± 0.010			

Table 5.7. Frequency-domain analysis results of the PSD_θ variable.

PSD_α	Groups	mean ± sd	Statistics	p-value	P_k
RSS	{2,3,4,5}	0.096 ± 0.013	Trial 1 {2,3,4,5}vs{6}	1.47E-120	0.788
	{3,4,5}	0.099 ± 0.012	Trial 2 {3,4,5}vs{6}	9.32E-83	0.748
	{4,5}	0.099 ± 0.011	Trial 3 {4,5}vs{6}	3.14E-29	0.664
	{5}	0.105 ± 0.010	Trial 4 {5}vs{6}	7.08E-10	0.613
	{6}	0.109 ± 0.010			
GAG	{0}	0.101 ± 0.013	GAG {0} vs {1}	3.29E-16	0.741
	{1}	0.090 ± 0.012			

Table 5.8. Frequency-domain analysis results of the PSD_α variable.

PSD_β	Groups	mean ± sd	Statistics	p-value	P_k
RSS	{2,3,4,5}	0.370 ± 0.027	Trial 1 {2,3,4,5}vs{6}	1.66E-11	0.583
	{3,4,5}	0.374 ± 0.025	Trial 2 {3,4,5}vs{6}	0.011	0.533
	{4,5}	0.378 ± 0.025	Trial 3 {4,5}vs{6}	0.429[n.s.]	0.512
	{5}	0.379 ± 0.024	Trial 4 {5}vs{6}	0.118[n.s.]	0.529
	{6}	0.377 ± 0.024			
GAG	{0}	0.377 ± 0.028	GAG {0} vs {1}	3.54E-05	0.622
	{1}	0.366 ± 0.029	*n.s. statistically non-significant level*		

Table 5.9. Frequency-domain analysis results of the PSD$_\beta$ variable.

PSD_{TB}	Groups	mean ± sd	Statistics	p-value	P_k
RSS	{2,3,4,5}	0.894 ± 0.043	Trial 1 {2,3,4,5}vs{6}	7.69E-24	0.624
	{3,4,5}	0.899 ± 0.042	Trial 2 {3,4,5}vs{6}	4.27E-12	0.589
	{4,5}	0.905 ± 0.042	Trial 3 {4,5}vs{6}	1.75E-3	0.546
	{5}	0.907 ± 0.040	Trial 4 {5}vs{6}	0.185[n.s.]	
	{6}	0.909 ± 0.043			
GAG	{0}	0.901 ± 0.047	GAG {0} vs {1}	3.67E-4	0.605
	{1}	0.887 ± 0.044	*n.s. statistically non-significant level*		

Table 5.10. Frequency-domain analysis results of the PSD_{TB} variable.

5.2. Symbolic dynamic results

5.2.1. Classifying groups by single variables

The following Tables 5.11 and 5.12 present the number of variables obtained from the symbolic dynamics methodology that are able to classify the studied groups in the different trial sets. The best variables are characterized with *p-value*<0.0005, *Sen*>60%, *Spe* >60% and P_k >0.6 and the number of variables that met this condition appear in first place in each cell of the Tables 5.11 and 5.12. The second number corresponds to the number of variables that showed a *p-value*<0.0005 and P_k >0.6. The Bonferroni correction was used to adjust the significant level (*p-value*<6.88E-06*)* due to the high number of variables proposed. In Table 5.11, it should be noticed that the variables in the α band have

low impact influence in the discrimination between the groups. The influence of variables in the θ band only appear in trial 1 (RSS={2,3,4,5}vs RSS={6}) but also with low influence impact. This behavior could be explained by the effect of slow activity in θ band and because the closed eyes in α band in all studied groups. Related to TB and All bands, a higher number of variables can be found in TB band rather than All band (see Table 5.12). For this reason, TB band is used in the present project for studying the contribution of the proposed variables in the complete frequency range in order to predict nociceptive stimuli responses.

Frequency band	trial 1	trial 2	trial 3	trial 4	GAG
α	0/7	0/6	0/2	0/0	0/0
β	70/203	16/156	0/13	0/0	0/31
δ	45/142	9/100	0/6	0/3	0/2
θ	0/116	0/0	0/0	0/0	0/0

Table 5.11. Number of variables able to classify the trial groups in the traditional frequency bands.

Frequency band	trial 1	trial 2	trial 3	trial 4	GAG
All	245/385	153/303	3/134	0/35	0/15
TB	247/381	170/308	6/143	0/39	0/20

Table 5.12. Number of variables able to classify the trial groups in the All Spectrum and Total band.

In next subsections, the results concerning to the different trials are presented. The best values of the variables with *p-value*<0.0005, *Sen*>60%, *Spe* >60% and P_k >0.6 were taken into account.

TRIAL 1

Trial 1 studies the statistical differences of RSS={2,3,4,5} vs RSS={6} with *p-value* $< 6.88E\text{-}6$, $Spe > 60\%$, $Sen > 60\%$ and $P_k > 0.6$. In this study, the symbol defined variables in NEQ algorithm present the best statistical differences in the β band, as seen in Table 5.13. The variables which obtained highest P_k were w133, with a value of 0.708, and $F1$ with a value of 0.725. Higher P_k values of the variables $w133$ and $F1$ are observed in the RSS={2,3,4,5} group rather than in the RSS={6} group, denoting a higher probability of occurrence in RSS={2,3,4,5} group. This means that variables $w133$ and $F1$ are more probable to appear in the signals of group RSS={2,3,4,5}. However, the RSS={6} group of the variable $sF0_u$ has a greater mean value than the RSS={2,3,4,5} group. Bearing in mind the nature of $F1$ variable, $F1$ measures the probability of experimenting one change in a symbol of the EEG signals, which means that the RSS={2,3,4,5} group implies more variations. Furthermore, this can also be explained by giving an interpretation of $sF0_u$, which measures the probability of no variations in the symbols, that is to say, RSS={6} group implies minor number of symbol changes. In the β band, the lower variability behavior of the variables are observed in RSS={6} group as denoted by the entropy $HqsF(6)$. This noted tendency (*p-value* = 3.52E-36) could confirm a higher regularity of the EEG signal behavior in RSS={6} group.

In Fig. 5.1, the function of variable $w133$ in relation to parameter a is shown, showing a decreasing tendency of $w133$ values as a increases. The best statistical differences correspond to $a=0.025$.

Band	Algorithm	Parameter a	Variable	RSS={2,3,4,5} mean ± sd	RSS={6} mean ± sd	*p-value*	P_k
β	NEQ_Families	**0.0875**	**$F1$**	**0.540 ± 0.031**	**0.517 ± 0.022**	**1.15E-74**	**0.725**
		0.125	$sF0_u$	0.204 ± 0.041	0.232 ± 0.035	1.98E-60	0.702
	NEQ_words	0.025	$w133$	0.096 ± 0.014	0.086 ± 0.012	2.96E-64	0.708
	EQ_Families	-	$HqsF(6)$	2.01 ± 0.370	1.82 ± 0.343	3.52E-36	0.655

Table 5.13. Results of the variables that best classified the two studied groups in trial 1 in the β band.
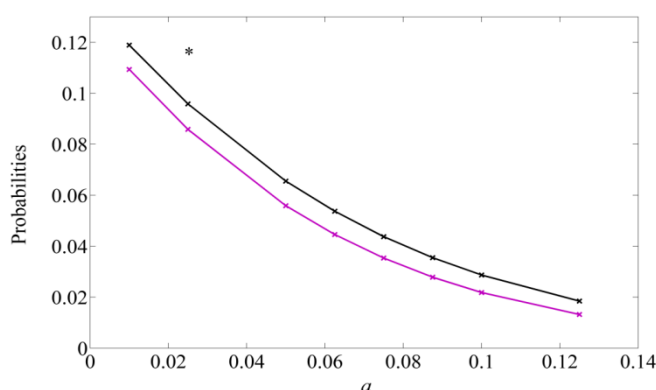
Fig. 5.1. The mean of the $w133$ obtained for different values of the parameter a and the β band. The RSS={2,3,4,5} group is represented by the black line and the RSS={6} group by the magenta line. * The marked parameter stands out for performing the following results: $p\text{-}value < 6.88E\text{-}6, Spe > 60\%, Sen > 60\%$ and $P_k > 0.6$.

In δ band (Table 5.14), the best results were obtained using a NEQ algorithm. Rényi entropies confirm the high regularity (low variability) in RSS={6} group with a P_k=0.717 for Hqw with q=0.4. Additionally, the function of variable Hqw in relation to parameter q is presented in Fig. 5.2. It can be observed that Hqw diminishes with the increasing values of parameter q. Nevertheless, the best statistical results correspond to $q<0.7$.

Band	Algorithm	Parameter a	Variable	RSS={2,3,4,5} mean ± sd	RSS={6} mean ± sd	*p-value*	P_k
δ	NEQ_levels	0.0875	$Hql(3)$	1.79 ± 0.171	1.70 ± 0.177	7.09E-37	0.656
	NEQ_words	**0.025**	**$Hqw(0.4)$**	**3.71 ± 0.104**	**3.66 ± 0.112**	**2.23E-69**	**0.717**

Table 5.14. Results of the variables that best classified the two studied groups in trial 1 in the δ frequency band.
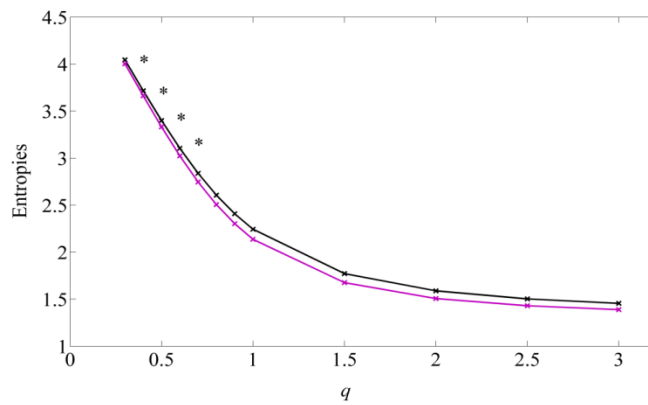
Fig. 5.2. The mean of the Hqw obtained for different values of the parameter q and the δ band (a=0.025). The RSS={2,3,4,5} group is represented by the black line and the RSS={6} group by the magenta line. *The marked parameters stand out for performing the following results: *p-value* < 6.88E-6, $Spe > 60\%$, $Sen > 60\%$ and $P_k > 0.6$.

Band	Algorithm	Parameter a	Variable	RSS={2,3,4,5} mean ± sd	RSS={6} mean ± sd	*p-value*	P_k
TB	NEQ_Families	0.01	$HqsF(0.5)$	2.51 ± 0.143	2.41 ± 0.107	1.73E-73	0.723
			$HqF(0.9)$	1.21 ± 0.093	1.14 ± 0.074	1.76E-71	0.720
		0.1	$sF1_{de}$	0.076 ± 0.014	0.067 ± 0.011	1.78E-62	0.705
		0.125	$F0$	0.380 ± 0.094	0.435 ± 0.064	6.76E-58	0.698
			$F1$	0.424 ± 0.050	0.40 ± 0.039	7.92E-36	0.654
			$sF0_u$	0.380 ± 0.094	0.435 ± 0.064	6.76E-58	0.698
			$sF2_{du}$	0.088 ± 0.019	0.077 ± 0.015	3.28E-55	0.693
	NEQ_words	0.0625	$fw(0.0005)$	6.83 ± 6.46	13.3 ± 6.21	1.15E-99	0.760
		0.075	**$Hqw(0.2)$**	**5.58 ± 0.147**	**5.44 ± 0.134**	**7.55E-104**	**0.766**
		0.0875	$w\,221$	3.90E-3 ±1.67E-3	2.70E-3 ± 1.27E-3	3.54E-73	0.723
		0.1	$w\,003$	4.08E-3 ± 1.80E-3	2.73E-3 ± 1.40E-3	8.57E-82	0.736

Table 5.15. Results of the variables that best classified the two studied groups of trial 1 in the Total band.

NEQ algorithm permits to better describe RSS={2,3,4,5} and RSS={6} groups in TB band. Observing the values of the variables in TB band (Table 5.15), their behavior clearly denotes a higher regularity in RSS={6} group. In this way, the values of $sF1_{de}$, $F1$, $sF2_{du}$, $HqsF$ and HqF variables are higher in RSS={2,3,4,5} group than RSS={6} and the values of $F0$, $sF0_u$ are lower, which measures the probability to find the same symbols in the EEG signal. The variable with greatest P_k was $Hqw(0.2)$ with P_k= 0.766.

The performances of entropy $Hqw(0.2)$ and the number of forbidden words $fw(0.0005)$ function of parameter the a are shown from Fig. 5.3 and 5.4, respectively. Values of $a > 0.05$ presents statistical differences for entropy $Hqw(0.2)$ and values of $0.05 < a < 0.1$ for variable $fw(0.0005)$.

Fig. 5.3. The mean of the $Hqw(0.2)$ obtained for different values of the parameter a and the Total band (q=0.2). The RSS={2,3,4,5} group is represented by the black line and the RSS={6} group by the magenta line. * The marked parameters stand out for performing the following results: *p-value* $< 6.88\text{E-}6$, $Spe > 60\%$, $Sen > 60\%$ and $P_k > 0.6$.
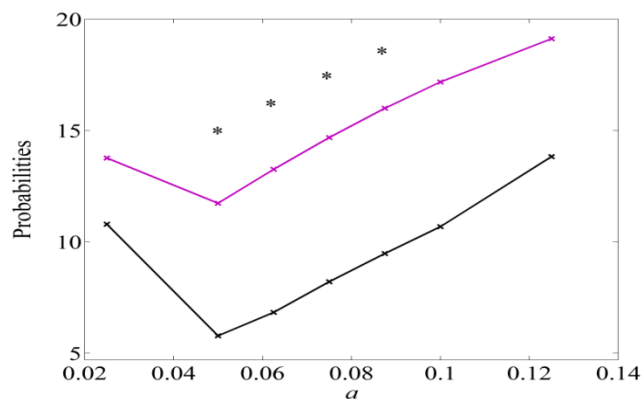
Fig. 5.4. The mean of the $fw(0.0005)$ obtained for different values of the parameter a and the Total band. The RSS={2,3,4,5} group is represented by the black line and the RSS={6} group by the magenta line. * The marked parameters stand out for performing the following results: *p-value* $< 6.88\text{E-}6$, $Spe > 60\%$, $Sen > 60\%$ and $P_k > 0.6$.

Moreover, the function of variable Hqw in relation to parameter q is presented in Fig. 5.5. It can be observed that Hqw diminishes with the increasing values of parameter q. Nevertheless, the best statistical results correspond to $q\leq1$.

Fig. 5.5. The mean of the Hqw obtained for different values of the parameter q and the Total band (a=0.075). The RSS={2,3,4,5} group is represented by the black line and the RSS={6} group by the magenta line. * The marked parameters stand out for performing the following results: $p\text{-}value <$ 6.88E-6, $Spe > 60\%$, $Sen > 60\%$ and $P_k > 0.6$.

TRIAL 2

Trial 2 studies the statistical differences of RSS={3,4,5} vs RSS={6} with $p\text{-}value < 6.88E\text{-}6$, $Spe > 60\%$, $Sen > 60\%$ and $P_k > 0.6$. In this study, the symbol defined variables in NEQ algorithm present the best statistical differences. In Table 5.16, it can be noticed that $sF1_{ed}$ and $sF1_{ue}$ variables, that contain a variation in the symbol sequence, present a higher value in RSS={3,4,5} group in β band. Since the RSS={3,4,5} tends to have a greater variability of their symbols, it can be stated that these two variables gather the complexity behavior contained in RSS={3,4,5} group in contrast with RSS={6} group. The best statistical differences were found in $w133$ variable (P_k=0.688) which captures the highest symbol variability. The RSS={3,4,5} group sets out a higher mean value than RSS={6}, indicating that RSS={3,4,5} group has the greatest complexity.

The behavior of the variable $w133$ in function of parameter a is shown in Fig. 5.6. The value of $w133$ decreases with the increasing of parameter a. The best statistical differences correspond to a=0.025.

Band	Algorithm	Parameter a	Variable	RSS={3,4,5} mean ± sd	RSS={6} mean ± sd	$p\text{-}value$	P_k
β	NEQ_Families	0.1	$sF1_{ed}$	0.173 ± 0.006	0.169 ± 0.006	1.16E-37	0.665
			$sF1_{ue}$	0.173 ± 0.006	0.169 ± 0.006	1.17E-39	0.669
	NEQ_words	**0.025**	**$w133$**	**0.095 ± 0.014**	**0.086 ± 0.012**	**1.29E-48**	**0.688**
		0.125	$fw(0.001)$	21.71 ± 2.0	22.76 ± 2.16	4.67E-29	0.640

Table 5.16. Results of the variables that best classified the two studied groups in trial 2 in the β band.

Fig. 5.6. The mean of the $w133$ obtained for different values of the parameter a and the β band. The RSS={3,4,5} group is represented by the black line and the RSS={6} group by the magenta line.* The marked parameters stand out for performing the following results: $p\text{-}value < 6.88\text{E-}6$, $Spe > 60\%$, $Sen > 60\%$ and $P_k > 0.6$.

For δ band, the best results were obtained using a NEQ algorithm. It can be observed in Table 5.17 that the entropy values in the RSS={3,4,5} group is considerably higher rather than in RSS={6} group, denoting a higher regularity in RSS={6} group. This shows a higher regularity in RSS={6}. The best statistical differences were found in $Hqw(0.4)$ for a=0.025. In this way, Fig. 5.7 shows the behavior of Hqw in function of parameter q. It is observed that the best P_k values are obtained for low values of q parameter.

Band	Algorithm	Parameter a	Variable	RSS={3,4,5} mean ± sd	RSS={6} mean ± sd	p-value	P_k
	NEQ_words	**0.025**	$Hqw(0.4)$	**3.71 ± 0.097**	**3.66 ± 0.112**	**6.19E-49**	**0.689**
δ	NEQ_levels	0.0875	$Hql(3)$	1.78 ± 0.171	1.70 ± 0.177	1.22E-24	0.632

Table 5.17. Results of the variables that best classified the two studied groups in trial 2 in the δ band.

Fig. 5.7. The mean of the Rényi entropy Hqw obtained for different values of the parameter q and the δ band. The RSS={3,4,5} group is represented by the black line and the RSS={6} group by the magenta line. * The marked parameters stand out for performing the following results: $p\text{-}value < 6.88\text{E-}6$, $Spe > 60\%$, $Sen > 60\%$ and $P_k > 0.6$.

The best results in TB band for Trial 2 also were obtained using NEQ algorithm, as it is seen in Table 5.18. The higher regularity is also presented in RSS={6} group. This behavior is stated by the entropies $HqF(2.5)$, $HqsF(0.1)$, $Hqw(0.2)$ which values are higher in RSS={3,4,5} group. Since the variables $F1$ and $w133$ express symbol variability also confirms this regularity previously observed in RSS={6} group. The number of forbidden words $fw(0.0005)$ are higher in RSS={6} group with $P_k = 0.730$. The best result was obtained by entropy $Hqw(0.2)$ with $P_k = 0.737$.

Band	Algorithm	Parameter a	Variable	RSS={3,4,5} mean ± sd	RSS={6} mean ± sd	p-value	P_k
TB	NEQ_Families	0.01	$HqF(2.5)$	0.985 ± 0.133	0.894 ± 0.109	2.55E-60	0.710
		0.125	$F1$	0.426 ± 0.047	0.40 ± 0.039	5.66E-37	0.663
			$HqsF(0.1)$	3.12 ± 0.02	3.11 ± 0.017	8.36E-64	0.717
	NEQ_words	0.01	$w133$	0.076 ± 0.020	0.064 ± 0.014	2.27E-52	0.696
		0.0625	$fw(0.0005)$	7.70 ± 6.490	13.3 ± 6.21	5.50E-72	0.730
		0.075	**$Hqw(0.2)$**	**5.57 ± 0.144**	**5.44 ± 0.134**	**7.46E-76**	**0.737**

Table 5.18. Results of the variables that best classified the two studied groups in trial 2 in the Total band.

The performance of entropy Hqw, with parameter a=0.075, in function of parameter q can be observed in Fig. 5.8. The values of the entropy decrease with the increasing values of q. Statistical significant values were found by q<0.7.
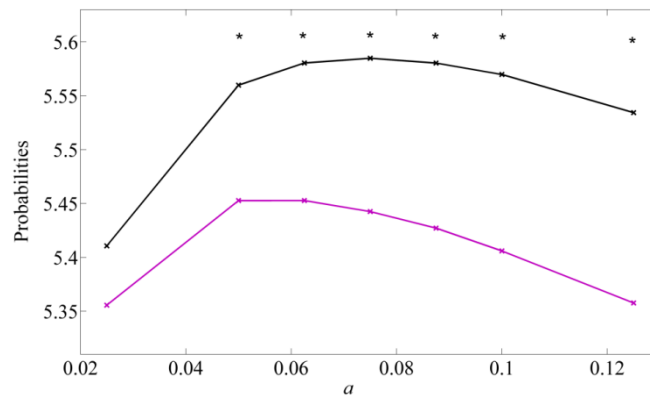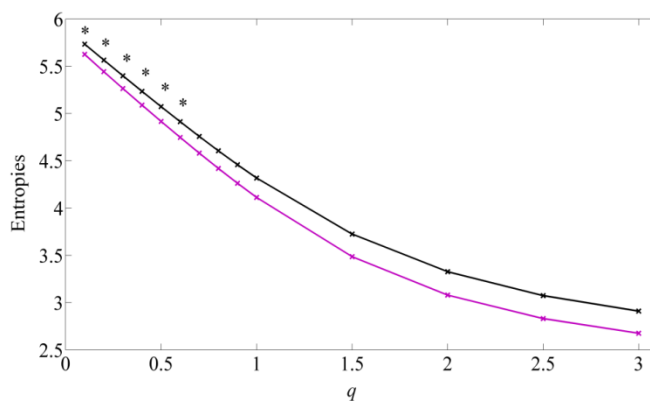

Fig. 5.8. The mean of the Rényi entropy Hqw obtained for different values of the parameter q and the Total band. The RSS={3,4,5} group is represented by the black line and the RSS={6} group by the magenta line.* The marked parameters stand out for performing the following results: *p-value* < 6.88E-6, $Spe > 60\%$, $Sen > 60\%$ and $P_k > 0.6$.
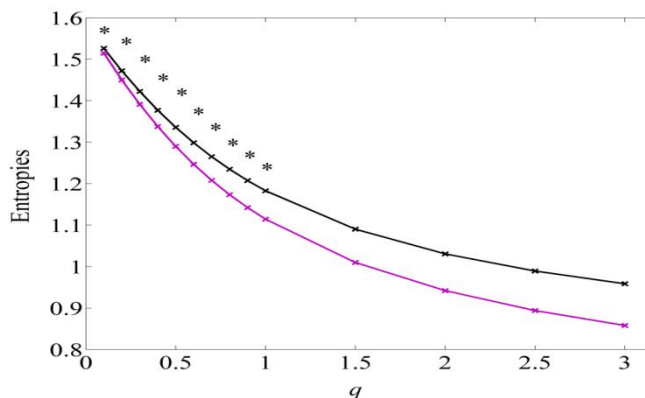
TRIAL 3

Trial 3 studies the statistical differences of RSS={4,5} vs RSS={6} with *p-value* $< 6.88E\text{-}6$, $Spe >$ 60%, $Sen > 60\%$ and $P_k > 0.6$. In this study, the symbolic defined variables in NEQ algorithm present the best statistical differences, but only in TB band as can be seen in Table 5.19. Variables $sF2_{du}$ and $w311$ state that higher variability is found in RSS={4, 5} group, thus a higher regularity RSS={6} group. The number of variables with probability higher than 0.3 and number of forbidden words were larger in RSS={6} group, with highest statistically differences in $fw(0.0005)$, $P_k =$ 0.649.

Band	Algorithm	Parameter a	Variable	RSS={4, 5} mean ± sd	RSS={6} mean ± sd	*p-value*	P_k
TB	NEQ_Families	0.125	$sF2_{du}$	0.084 ± 0.016	0.077 ± 0.015	1.01E-23	0.646
	NEQ_words	0.025	w 311	0.055 ± 0.017	0.047 ± 0.015	4.22E-23	0.644
			$pw(0.3)$	0.685 ± 0.893	1.08 ± 0.931	4.47E-17	0.611
		0.05	$fw(0.0005)$	**8.45 ± 6.11**	**11.7 ± 6.20**	**1.56E-24**	**0.649**

Table 5.19. Results of the variables that best classified the two studied groups in trial 3 in the Total band.

Fig. 5.9 presents the $w311$ variable behavior in function of parameter a. The values of $w311$ decrease with increasing values of a. The unique value with statistical significance level (*p-value* $< 6.88E\text{-}6$, $Spe > 60\%$, $Sen > 60\%$ and $P_k > 0.6$) corresponds to $a = 0.025$.
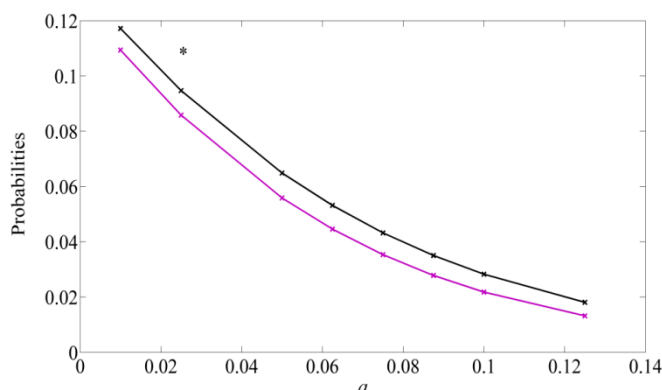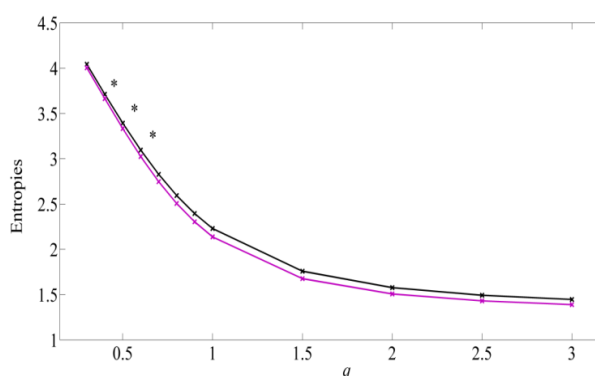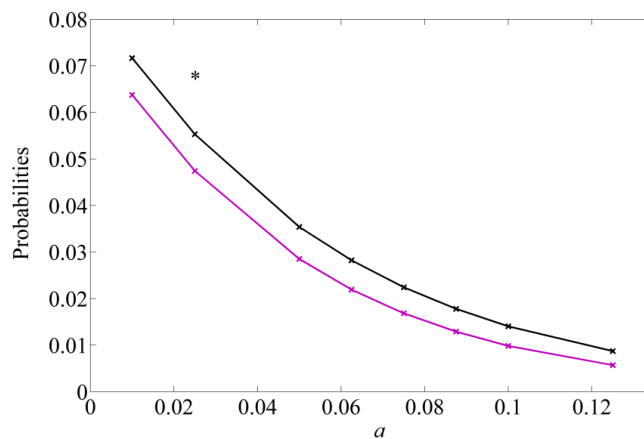

Fig. 5.9. The mean of the $w311$ obtained for different values of the parameter a and the Total band. The RSS={4,5} group is represented by the black line and the RSS={6} group by the magenta line.* The marked parameters stand out for performing the following results: *p-value* $< 6.88E\text{-}6$, $Spe >$ 60%, $Sen > 60\%$ and $P_k > 0.6$.

TRIAL 4

Trial 4 and trial 3 were the most difficult to discriminate the studied groups. Trial 4 studies the statistical differences of RSS={5} vs RSS={6} with only *p-value*<6.88E-6 and $P_k > 0.6$. In this trial, both EQ and NEQ algorithms of symbolic dynamics discriminate between groups but only in the TB band and with *p-value*<6.88E-6 and $P_k > 0.6$. Besides that, the mentioned trials could statistical differentiate with $p\text{-}value < 6.88E\text{-}6, Spe > 60\%, Sen > 60\%$ and $P_k > 0.6$.

The results from the algorithm based on EQ levels can be seen in Fig. 5.10 and Fig. 5.11. Also as it was observed in the other trials, states of the patient with more stimuli responses (RSS<6) present more complexity than state without stimuli response (RSS=6). This behavior is followed by each of the defined variables seen in Fig. 5.10, where values of the variables tend to be higher in RSS={5} group than in RSS={6} group. This behavior is also confirmed by the $HqsF(0.1)$ variable, which emphasizing the lower probabilities of subfamily patterns (q<1), because RSS={5} group has a higher value that indicates higher complexity. The best results were obtained by $F2du$ and $F2ud$ that reached a P_k value of 0.6 and 0.607, respectively.

While Fig. 5.10 contains the results of subfamilies patterns, Fig. 5.11 shows the results of the words that best could differentiate RSS={5} and RSS={6} groups. Values of entropy $Hqw(0.1)$ were higher in RSS={5} group that indicates higher complexity.
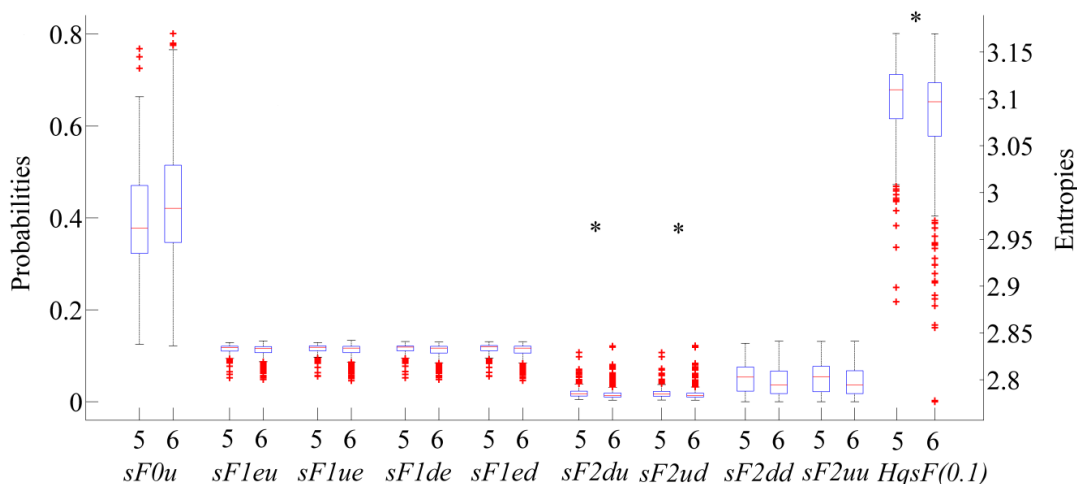
Fig. 5.10. The probabilities and entropies of the Subfamily patterns are studied in the Total band using the EQ algorithm. *The variables marked stand out for performing the following results: *p-value* < 6.88E-6 and $P_k > 0.6$.
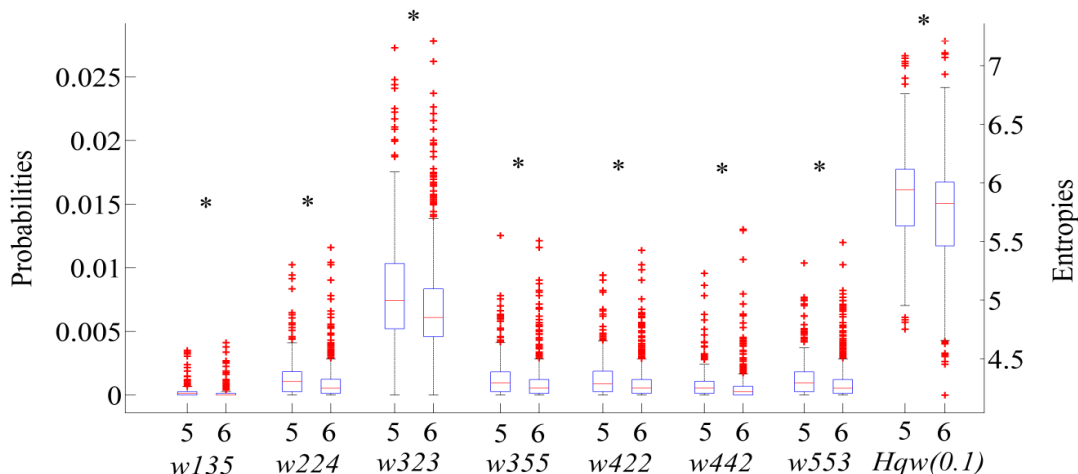
Fig. 5.11. The probabilities and entropies of words are studied in the Total band using the EQ algorithm. *The variables marked stand out for performing the following results: *p-value* < 6.88E-6 and $P_k > 0.6$. The pattern which has a greater occurrence probability is the word *w323*.

The best results from the algorithm based on NEQ levels are listed in Table 5.20. The tendency of a greater mean value in the RSS={5} group, observed in previous tables, is also appreciated in this Table 5.20. An example of this behavior is the variable $Hqw(0.3)$ that shows a higher level of complexity in the RSS={5} group. It is interesting to notice that, in all cases, the RSS={5} state presents a higher symbol variability ($F1$, $sF1_{de}$, $sF1_{eu}$, $w331$). This tendency can also be obtained from the entropy variable $Hqw(0.1)$. As it is well-known, the entropy is a measure of unpredictability of information content. With this in mind, it can be stated that RSS={6} state is more regular.

The best results were obtained by *w331* with P_k=0.621 and with *a*=0.025, as it can be seen in Fig. 5.12.

Band	Algorithm	Parameter *a*	Variable	RSS={5} mean ± sd	RSS={6} mean ± sd	*p-value*	P_k
TB	NEQ_Families	0.01	$F1$	0.328 ± 0.053	0.311 ± 0.051	3.71E-08	0.601
			$sF1_{de}$	0.076 ± 0.013	0.071 ± 0.013	1.5E-09	0.611
			$sF1_{eu}$	0.076 ± 0.014	0.071 ± 0.013	1.9E-09	0.610
	NEQ_words	**0.025**	**$w331$**	**0.053 ± 0.015**	**0.047 ± 0.015**	**5.04E-11**	**0.621**
		0.125	$fw(0.005)$	31.1 ± 4.16	32.5 ± 4.44	2.57E-09	0.609
			$Hqw(0.3)$	5.28 ± 0.176	5.22 ± 0.182	2.07E-10	0.617

Table 5.20. Results of the variables that best classified the two studied groups in trial 4 in the Total band.
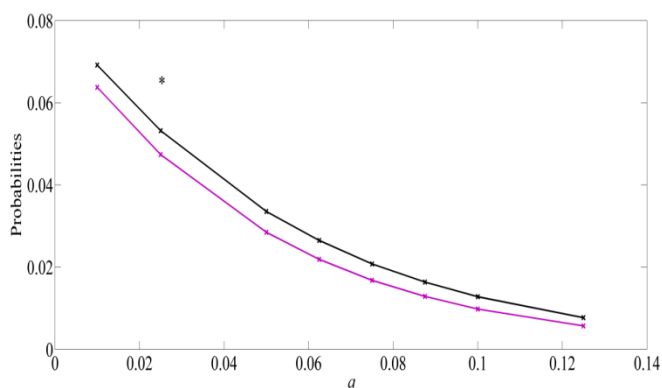
Fig. 5.12. The mean of the w331 obtained for different values of the parameter a in the Total band and for the NEQ algorithm. The RSS={5} group is represented by the black line and the RSS={6} group by the magenta line. * The marked parameter stands out for performing a *p-value* < 6.88E-6 and

$$P_k > 0.6.$$

GAG STUDY

The best results with statistical significant differences (with *p-value* < 6.88E-6, $Spe > 60\%$, $Sen > 60\%$ and $P_k > 0.6$) between GAG={0} and GAG={1} are contain in Table 5.21. Only NEQ algorithm could offer the best results. In this study, the nociceptive stimuli response (GAG={1}) as well shows higher complexity compared to non-response state (GAG={0}). This behavior was followed by w 133 and $sF1_{eu}$ in the β band. Similarly, this tendency is adopted by entropies $HqsF(0.3)$ and $Hqw(0.20)$. Variable $pw(0.025)$ could differentiate both groups in the δ band, and $fw(0.001)$ in the TB band. Finally, $sF1_{eu}$ was the best classifier of the groups RSS={5} and RSS={6} with P_k=0.756.

Band	Algorithm	Parameter a	Variable	GAG=0 mean ± sd	GAG=1 mean ± sd	*p-value*	P_k
β	NEQ_words	0.01	w 133	0.114±0.012	0.126±0.012	7.60E-18	0.754
	NEQ_Families	0.01	**$sF1_{eu}$**	**0.124±0.011**	**0.135±0.012**	**4.38E-18**	**0.756**
			$HqsF(0.3)$	1.77±0.202	1.94±0.209	2.70E-14	0.725
δ	NEQ_words	0.025	$pw(0.025)$	2.67±0.902	3.21±0.927	1.29E-8	0.648
TB	NEQ_words	0.05	$Hqw(0.20)$	5.51±0.175	5.61±0.108	5.85E-16	0.739
			$fw(0.001)$	14.82±7.85	8.16±7.24	1.01E-16	0.745

Table 5.21. Results of the variables that best classified the two studied groups of GAG in different frequency bands.

5.2.2. Detection of the RSS states by multivariable functions

A further study was performed combining the best non-linear variables obtained with variables from time-domain, frequency-domain and also from clinical information. New variables were constructed using two variables (a multivariable function) for each of them. These multivariable functions enable to achieve a greater prediction probability. Table 5.22 shows the goodness of the new created multivariable functions, tested in each four trials. Score 1 means that the evaluated function had a *p-value*<0.0005, *Sen*>60%, *Spe* >60% and P_k >0.6 for a certain trial. Score 0 means that the function could not perform a trial. The best multivariable functions are those containing score 1 in the four trials. Table 5.23 contains the statistical parameters (*Sen*/*Spe*/P_k) obtained from those multivariable functions with score 1 in all the trials. The new variable *f(SD, TB_NEQ_words_0.075_Hqw(0.2))* could better perform states in trial 4 compared to clinical indexes (*BIS* and *AAI*).

Variables	trial 1	trial 2	trial 3	trial 4
Ce_{remi} PSD_δ	1	0	0	1
PSD_δ SD	1	1	0	1
PSD_δ *TB_NEQ_words_0.125_Hqw(0.3)*	1	1	0	1
PSD_δ **β_NEQ_words_0.025_w133**	**1**	**1**	**1**	**1**
PSD_{TB} *TB_NEQ_words_0.025_w331*	1	1	0	1
PSD_{TB} *TB_NEQ_words_0.025_w311*	1	1	0	1
SD **TB_NEQ_words_0.025_w331**	**1**	**1**	**1**	**1**
SD **TB_NEQ_words_0.125_Hqw(0.3)**	**1**	**1**	**1**	**1**
SD **TB_NEQ_words_0.025_w311**	**1**	**1**	**1**	**1**
SD *TB_NEQ_words_0.01_w133*	1	1	0	1
SD **TB_NEQ_words_0.075_Hqw(0.2)**	**1**	**1**	**1**	**1**
TB_NEQ_Families_0.01_F1 *TB_NEQ_words_0.025_w331*	0	0	0	1
TB_NEQ_Families_0.01_F1 *TB_NEQ_words_0.025_w311*	0	0	0	1
TB_NEQ_Families_0.01_F1de *TB_NEQ_words_0.025_w311*	0	0	0	1
TB_NEQ_Families_0.01_F1eu *TB_NEQ_words_0.025_w311*	0	0	1	1

*TB_NEQ_words*_0.025_*w*331	0	1	0	1
*TB_NEQ_words*_0.01_*w*133				
*TB_NEQ_words*_0.025_*w*331	0	1	0	1
*TB_NEQ_Families*_0.01_*HqF(0.5)*				
*TB_NEQ_words*_0.025_*w*331	0	1	0	1
*TB_NEQ_Families*_0.01_*HqF(0.9)*				
TB_NEQ_words_0.025_w331	**1**	**1**	**1**	**1**
TB_NEQ_words_0.0875_w122				
TB_NEQ_words_0.025_w331	**1**	**1**	**1**	**1**
TB_NEQ_words_0.0875_w221				
*TB_NEQ_words*_0.025_*w*331	1	1	0	1
*TB_NEQ_words*_0.1_*w*122				
*TB_NEQ_words*_0.01_*w*133	0	1	0	1
*TB_NEQ_Families*_0.125_*F0*				

Table 5.22. Further study combining linear and non-linear variables to construct a new one.

Sen/Spe/P_k	trial 1	trial 2	trial 3	trial 4
PSD_δ *β_NEQ_words*_0.025_*w*133	63.7/ 70.3/ 0.717	69.9/ 63.5/ 0.713	63.9/ 60.4/ 0.663	60.0/ 60.6/ 0.623
SD *TB_NEQ_words*_0.025_*w*331	60.1/ 67.3/ 0.680	66.4/ 60.7/ 0.675	62.1/ 60.0/ 0.641	60.3/ 61.4/ 0.637
SD *TB_NEQ_words*_0.125_*Hqw(0.3)*	66.7/ 75.8/ 0.763	73.7/ 65.6/ 0.737	67.8/ 62.6/ 0.678	**62.5/** **64.3/** **0.659**
SD *TB_NEQ_words*_0.025_*w*311	60.0/ 66.9/ 0.680	66.2/ 60.9/ 0.675	62.3/ 60.0/ 0.641	60.0/ 61.0/ 0.636
SD **TB_NEQ_words_0.075_Hqw(0.2)**	**69.4/** **77.2/** **0.790**	**73.1/** **67.0/** **0.758**	**66.5/** **61.8/** **0.687**	**60.8/** **63.9/** **0.656**
*TB_NEQ_words*_0.025_*w*331 *TB_NEQ_words*_0.0875_*w*122	60.8/ 70.6/ 0.688	71.0/ 61.7/ 0.698	63.8/ 60.2/ 0.654	60.3/ 60.4/ 0.622
*TB_NEQ_words*_0.025_*w*331 *TB_NEQ_words*_0.0875_*w*221	60.4/ 69.7/ 0.684	70.3/ 61.3/ 0.695	62.9/ 60.7/ 0.651	60.8/ 60.4/ 0.622

Table 5.23. RSS validation of the new constructed variables. Each of the cells of the table contains three values, which correspond to Sensitivity, Specificity and P_k, respectively (*Sen*/*Spe*/P_k).

5.2.3. Correlation of the single variables contained in the multivariable functions

Correlation analysis applied to the non-linear variables, selected as the best classifiers of the RRS states, are presented from Tables 5.24 to 5.27. In this way, Tables 5.24 and 5.25 contains the information relative to RSS={5} state, and Tables 5.26 and 5.27 the information relative to RSS={6}.

Table 5.24 includes the correlation between the non-linear variables, EEG standard deviation (*SD*) and clinical indexes. It is observed weak correlation between the couple *TB_NEQ_words*_0.025_*w*311 and *SD* (r_s=0.308), and between the couple *TB_NEQ_words*_0.0875_*w*122 and *SD* (r_s= -0.307). Higher correlations are presented when the non-linear variables are compared to variables obtained from power spectral density, as it is observed in Table 5.25. All non-linear variables are correlated to PSD_δ, PSD_θ, PSD_α. In this way, PSD_δ is highly correlated to *TB_NEQ_words*_0.025_*w*331 (r_s=-0.726) and to *TB_NEQ_words*_0.025_*w*311 (r_s=-0.725), PSD_θ is highly correlated to *TB_NEQ_words*_0.125_*Hqw*(0.3) (r_s=-0.723), and PSD_α is highly correlated to *TB_NEQ_words*_0.125_*Hqw*(0.3) (r_s=-0.714) and to *TB_NEQ_words*_0.075_*Hqw*(0.2) (r_s=-0.740). It needs to be emphasized the fact that these non-linear variables are correlated to those different bands that were calculated by. Furthermore, PSD_β and PSD_{TB} were not correlated to any of the non-linear variables.

Spearman's correlation/ *p-value*	*SD*	*AAI*	*BIS*	C_{propo}	C_{remi}
*β_NEQ_words*_0.025_*w*133	-0.258/ 6.91E-7	-4.60E-3/ n.s.	0.042/ n.s.	-0.073/ n.s.	0.071/ n.s.
*TB_NEQ_words*_0.025_*w*331	0.308/ 2.33E-9	-0.019/ n.s.	0.082/ n.s.	0.211/ 5.48E-5	-0.083/ n.s.
*TB_NEQ_words*_0.125_*Hqw*(0.3)	-0.079/ n.s.	-0.048/ n.s.	0.009/ n.s.	0.048/ n.s.	-0.016/ n.s.
*TB_NEQ_words*_0.025_*w*311	0.308/ 2.53E-9	-0.018/ 0.731	0.083/ n.s.	0.213/ 4.81E-5	-0.075/ n.s.
*TB_NEQ_words*_0.075_*Hqw*(0.2)	-0.255/ 9.51E-7	-0.059/ n.s.	-0.014/ n.s.	-0.036/ n.s.	1.41E-3/ n.s.
*TB_NEQ_words*_0.0875_*w*122	-0.307/ 2.78E-9	-0.044/ n.s.	-0.055/ n.s.	-0.076/ n.s.	0.019/ n.s.
*TB_NEQ_words*_0.0875_*w*221	-0.275/ 1.11E-7	-0.020/ n.s.	-0.051/ n.s.	-0.057/ n.s.	0.057/ n.s.

Table 5.24. Correlation between the non-linear variables, time-domain analysis and clinical indexes. These variables correspond to the RSS={5} state. n.s., non-significant statistical analysis.

Spearman's correlation/ p-value	PSD_δ	PSD_θ	PSD_α	PSD_β	PSD_{TB}
$\beta_NEQ_words_$0.025_w133	-0.349/ 9.09E-12	-0.568/ 4.12E-32	-0.617/ 3.37E-39	-0.049/ n.s.	-0.136/ 0.010
$TB_NEQ_words_$0.025_w331	**-0.726/ 3.14E-60**	-0.545/ 3.09E-29	-0.362/ 1.32E-12	0.279/ 7.16E-8	-0.135/ 0.010
$TB_NEQ_words_$0.125_Hqw(0.3)	-0.604/ 3.07E-37	**-0.723/ 2.24E-59**	**-0.714/ 2.02E-57**	-0.059/ n.s.	-0.191/ 2.70E-4
$TB_NEQ_words_$0.025_w311	**-0.725/ 6.69E-60**	-0.555/ 3.06E-29	-0.363/ 1.22E-12	0.276/ 9.95E-8	-0.137/ 9.05E-3
$TB_NEQ_words_$0.075_Hqw(0.2)	-0.489/ 4.75E-23	-0.693/ 9.45E-53	**-0.740/ 1.44E-63**	-0.120/ 0.023	-0.141/ 7.27E-3
$TB_NEQ_words_$0.0875_w122	-0.374/ 2.08E-13	-0.561/ 2.83E-31	-0.595/ 8.74E-36	-0.044/ n.s.	-0.050/ n.s.
$TB_NEQ_words_$0.0875_w221	-0.409/ 3.08E-13	-0.566/ 2.27E-30	-0.598/ 2.95E-35	-0.037/ n.s.	-0.042/ n.s.

Table 5.25. Correlation between the non-linear variables and frequency-domain analysis variables. These variables correspond to the RSS={5} state. n.s., non-significant statistical analysis.

Table 5.26 includes the correlation between the non-linear variables, EEG standard deviation (*SD*) and clinical indexes. It is observed weak correlation between the couple *TB_NEQ_words*_0.025_*w*331and *SD* (r_s=0.497), and between the couple *TB_NEQ_words*_0.025_*w*311 and *SD* (r_s= 0.495). Lower correlations were found in RSS={6} state than RSS={5} state when non-linear variables were compared to PSD_δ, PSD_θ, PSD_α, as it is observed in Table 5.27. In this manner by analyzing RSS={6} state, PSD_δ is strongly correlated to *TB_NEQ_words*_0.025_*w*331 (r_s= -0.617) and to *TB_NEQ_words*_0.025_*w*311 (r_s=-0.615), PSD_θ is strongly correlated to *TB_NEQ_words*_0.125_*Hqw*(0.3) (r_s=-0.617) and to *TB_NEQ_words*_0.075_*Hqw*(0.2) (r_s=-0.601), and PSD_α is strongly correlated to *TB_NEQ_words*_0.125_*Hqw*(0.3) (r_s=-0.595) and to *TB_NEQ_words*_0.075_*Hqw*(0.2) (r_s=-0.679). It needs to be emphasized the fact that these non-linear variables are correlated to those different bands that were calculated by.

The correlations of those non-linear variables that are combined in the best multivariable functions are contained in Table 5.28. The correlations in RSS={6} state and RSS={5} state are separately studied. It can be noted that these variables are weakly correlated, however, RSS={6} state presents lower correlations.

Spearman's correlation/ *p-value*	*SD*	*AAI*	*BIS*	C_{propo}	C_{remi}
*β_NEQ_words_*0.025_*w*133	-0.154/ 1.93E-5	0.024/ n.s.	0.045/ n.s.	-0.147/ 4.26E-5	0.129/ 3.47E-3
*TB_NEQ_words_*0.025_*w*331	0.497/ 5.68E-49	-2.36E-3/ n.s.	-0.025/ n.s.	0.171/ 1.97E-6	0.047/ n.s.
*TB_NEQ_words_*0.125_*Hqw(*0.3*)*	-0.037/ n.s.	0.065/ n.s.	0.049/ n.s.	-0.074/ 0.039	0.085/ 0.018
*TB_NEQ_words_*0.025_*w*311	0.495/ 1.71E-48	-0.007/ n.s.	-0.030/ n.s.	0.168/ 2.80E-6	0.050/ n.s.
*TB_NEQ_words_*0.075_*Hqw(*0.2*)*	-0.252/ 1.47E-12	0.097/ 7.0E-3	0.074/ 0.040	-0.174/ 1.29E-6	0.090/ 0.012
*TB_NEQ_words_*0.0875_*w*122	-0.285/ 8.78E-16	0.083/ 0.022	0.061/ n.s.	-0.210/ 4.61E-9	0.105/ 3.75E-3
*TB_NEQ_words_*0.0875_*w*221	-0.256/ 5.21E-17	0.076/ 0.035	0.088/ 1.50E-2	-0.197/ 4.08E-8	0.080/ 0.028

Table 5.26. Correlation between the non-linear variables, time-domain analysis and clinical indexes. These variables correspond to the RSS={6} state. n.s., non-significant statistical analysis.

Spearman's correlation/ *p-value*	PSD_δ	PSD_θ	PSD_α	PSD_β	PSD_{TB}
*β_NEQ_words_*0.025_*w*133	-0.116/ 1.26E-3	-0.304/ 7.44E-18	-0.411/ 1.56E-32	-0.055/ n.s.	0.014/ n.s.
*TB_NEQ_words_*0.025_*w*331	-0.617/ 1.37E-81	-0.507/ 4.20E-51	-0.218/ 1.14E-9	0.276/ 7.27E-15	-0.079/ 0.028
*TB_NEQ_words_*0.125_*Hqw(*0.3*)*	-0.407/ 7.53E-32	-0.617/ 2.0E-81	-0.595/ 1.41E-74	4.21E-4/ n.s.	-0.093/ 0.010
*TB_NEQ_words_*0.025_*w*311	-0.615/ 9.60E-81	-0.507/ 3.34E-51	-0.219/ 9.98E-10	0.276/ 7.01E-15	-0.077/ 0.032
*TB_NEQ_words_*0.075_*Hqw(*0.2*)*	-0.307/ 3.62E-18	-0.601/ 2.35E-76	-0.679/ 1.73E-104	-0.093/ 6.69E-3	-0.0879/ 0.015
*TB_NEQ_words_*0.0875_*w*122	-0.209/ 5.16E-9	-0.476/ 1.65E-44	-0.542/ 1.13E-59	-0.076/ 0.036	-6.88E-3/ n.s.
*TB_NEQ_words_*0.0875_*w*221	-0.222/ 5.07E-10	-0.480/ 2.43E-45	-0.545/ 1.60E-60	-0.055/ n.s.	-3.32E-3/ n.s.

Table 5.27. Correlation between the non-linear variables and frequency-domain analysis variables. These variables correspond to the RSS={6} state. n.s., non-significant statistical analysis.

Spearman's correlation/ *p-value*	RSS={5}	RSS={6}
*TB_NEQ_words*_0.025_*w*331	0.320/	0.272/
*TB_NEQ_words*_0.0875_*w*221	5.25E-10	1.04E-14
*TB_NEQ_words*_0.025_*w*311	0.333/	0.250/
*TB_NEQ_words*_0.0875_*w*122	1.07E-10	1.26E-12

Table 5.28. Spearman's correlation of the two single variables related to the multivariate functions.

5.2.4. Detection of the GAG states from multivariable functions

The study of the GAG reflex was also used as a validation method to discriminate if a patient is able to respond to noxious stimuli based on the best multivariable functions obtained from the study of RSS trials. In this way, Table 5.29 presents how these best multivariable functions performed the states in GAG. These multivariable functions are the same presented in Table 5.23. It can be stated that all these variables were able to detect GAG responses with a $P_k > 0.6$.

Variable	P_k
PSD_δ *β_NEQ_words*_0.025_*w*133	0.623
SD *TB_NEQ_words*_0.025_*w*331	0.637
SD *TB_NEQ_words*_0.125_*Hqw*(0.3)	0.659
SD *TB_NEQ_words*_0.025_*w*311	0.636
SD *TB_NEQ_words*_0.075_*Hqw*(0.2)	0.656
*TB_NEQ_words*_0.025_*w*331 *TB_NEQ_words*_0.0875_*w*122	0.622
*TB_NEQ_words*_0.025_*w*331 *TB_NEQ_words*_0.0875_*w*221	0.622

Table 5.29. GAG validation using the P_k index.

Chapter 6 and 7

Conclusions and future works

The present study has shown the scope of types of symbolic dynamics algorithms to the detection of the anesthesia states during minor surgery procedure. The methodology developed permitted to defined variables able to statistically differentiate sedation states during surgery: RSS={2,3,4,5} vs RSS={6} (trial 1), RSS={3,4,5} vs RSS={6} (trial 2), RSS={4,5} vs RSS={6} (trial 3), RSS={5} vs RSS={6} (trial 4) and GAG.

The two types of symbolic dynamics algorithms have been based on equidistant (EQ) and non-equidistant (NEQ) level distribution of the EEG signal. The methodology based on the EQ algorithm could only describe the evolution of the states in trial 4. Nevertheless, the methodology based on the NEQ algorithm could describe the evolution of the states in trials from 1 to 4, and also GAG.

More accurate analysis was obtained filtering the EEG signal in their characteristic frequency bands: δ, 0.1-4 Hz; θ, 4-8 Hz; α, 8-12 Hz; β, 12-30 Hz; TB (total frequency band); 0.1-45 Hz and ALL Spectrum, 0-45 Hz. In this way: trial 1 and trial 2 permitted variables to be defined in δ, β, TB bands; trial 3 and trial 4: only permitted variables to be defined in TB band.

The study of the parameters involved in the algorithms for better describing the behavior of the sedation states permitted to find the following parameter values a={0.025, 0.075} and q<1 for all the trials and GAG.

The defined variables could perform the different analyzed sedation states (RSS and GAG) with *p-value* $< 6.88E\text{-}6$, $Spe > 60\%$, $Sen > 60\%$ and $P_k > 0.6$. Similar tendencies were followed by those variables through all the trials, where more regularity was shown in RSS={6} state than the other states. Particularly, the values of $F0$, *pw* and *fw were higher in* RSS={6} state. Additionally, the values of the remaining variables were lower in RSS={6} state. Furthermore, the same defined multivariate functions (see Tables 5.23 and 5.29) could describe all RSS states and GAG states with $P_k > 0.6$.

Due to the methodology developed in the present project was an in-depth study, it offers new insights in depth of anesthesia prediction that could be used in other methodologies.

The precedent work could be applied in some interesting alternatives. Firstly, the presented study could be extended to other processing algorithms. Secondly, the best defined variables could be studied in different sample frequency rates of the EEG signal. Finally, a detector based on a multivariable function to asses sedation states during surgery procedures could be constructed.

Chapter 8

Environmental assessment

Given that the main objective of the present thesis is investigation and the only tools used to process the data are the one explained in the Methodology chapter, it can be stated that this project has a low environmental impact. It could be argued that the energy used during the algorithms' computation should have been taken into account, but at this point of the investigation this quantity has a minor impact on the project. The amount can be very small, however, it is important to emphasize that if a larger study with more patients is conducted, the execution time of the algorithms should be taken into account.

A larger study to increase the parameters range and improve the filter's characterization would multiply the number of combinations and thereby the computation time. The computer used for this study has a graphics chipset, a processor and an operating system which keeps running in the background. Assuming the hypothesis of implementing the current algorithms (conceived, for example, in C language) in recordable processing units where there is no need of hard disk nor screen, this could incur an important energy save and a simultaneous processing in different locations. As a general recommendation it could be used the computational architecture of RISC (Reduced Instruction Set Computing) that provides higher performance when combined with microprocessor architecture capable of executing instructions using fewer microprocessor cycles per instruction. Nevertheless, to run the C code in a device designed with this architecture, it is required a compiler to translate the C code into the microprocessor architecture.

Chapter 9

Project schedule

In this section of the thesis are listed the various phases of the project (planning, implementation and verification) and a temporal distribution (project's lifetime).

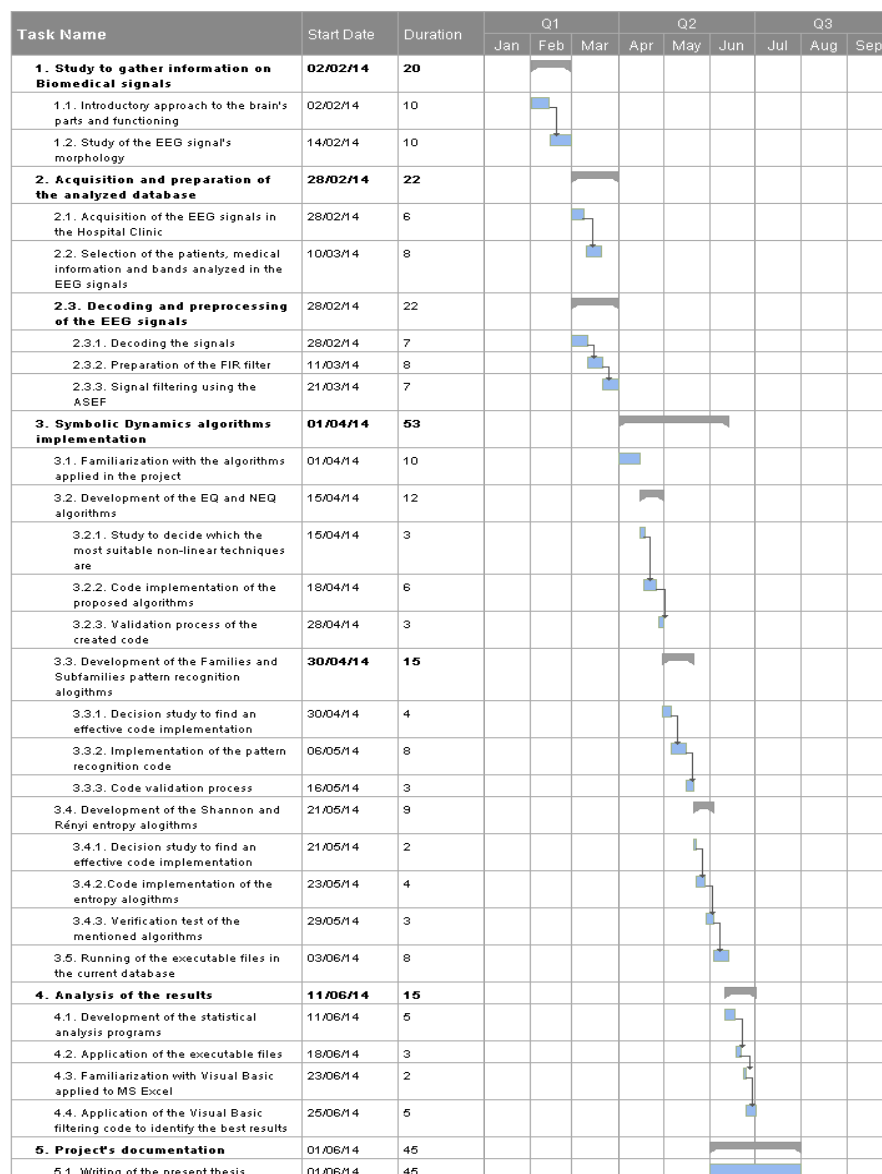| Task Name	Start Date	Duration	Q1			Q2			Q3		
			Jan	Feb	Mar	Apr	May	Jun	Jul	Aug	Sep
1. Study to gather information on Biomedical signals	**02/02/14**	**20**									
1.1. Introductory approach to the brain's parts and functioning	02/02/14	10									
1.2. Study of the EEG signal's morphology	14/02/14	10									
2. Acquisition and preparation of the analyzed database	**28/02/14**	**22**									
2.1. Acquisition of the EEG signals in the Hospital Clinic	28/02/14	6									
2.2. Selection of the patients, medical information and bands analyzed in the EEG signals	10/03/14	8									
2.3. Decoding and preprocessing of the EEG signals	28/02/14	22									
2.3.1. Decoding the signals	28/02/14	7									
2.3.2. Preparation of the FIR filter	11/03/14	8									
2.3.3. Signal filtering using the ASEF	21/03/14	7									
3. Symbolic Dynamics algorithms implementation	**01/04/14**	**53**									
3.1. Familiarization with the algorithms applied in the project	01/04/14	10									
3.2. Development of the EQ and NEQ algorithms	15/04/14	12									
3.2.1. Study to decide which the most suitable non-linear techniques are	15/04/14	3									
3.2.2. Code implementation of the proposed algorithms	18/04/14	6									
3.2.3. Validation process of the created code	28/04/14	3									
3.3. Development of the Families and Subfamilies pattern recognition alogithms	**30/04/14**	**15**									
3.3.1. Decision study to find an effective code implementation	30/04/14	4									
3.3.2. Implementation of the pattern recognition code	06/05/14	8									
3.3.3. Code validation process	16/05/14	3									
3.4. Development of the Shannon and Rényi entropy alogithms	21/05/14	9									
3.4.1. Decision study to find an effective code implementation	21/05/14	2									
3.4.2. Code implementation of the entropy alogithms	23/05/14	4									
3.4.3. Verification test of the mentioned algorithms	29/05/14	3									
3.5. Running of the executable files in the current database	03/06/14	8									
4. Analysis of the results	**11/06/14**	**15**									
4.1. Development of the statistical analysis programs	11/06/14	5									
4.2. Application of the executable files	18/06/14	3									
4.3. Familiarization with Visual Basic applied to MS Excel	23/06/14	2									
4.4. Application of the Visual Basic filtering code to identify the best results	25/06/14	5									
5. Project's documentation	**01/06/14**	**45**									
5.1. Writing of the present thesis	01/06/14	45									

Fig. 9.1. Gantt diagram of the project tasks.

Chapter 10

Budget

Because this is mostly a software project, there is not almost any material cost. However, in the following Table 10.1. are detailed all the material used for a successful execution of the project.

Material costs

Type of expenditure	Units	Unitary price [€/u]	Total [€]
Hardware			
HP 110-110es desktop computer	1	329.75	329.75
VS197DE ASUS Screen (18.5'')	1	61.98	61.98
Keyboard and mouse (Logitech Desktop Mk 120)	1	16.52	16.52
Software			
MATLAB 2014a license	1	8264.46	8264.46
Microsoft Office 2013 Professional's license (Word, Excel, Visio)	1	197.52	197.52
IBM SPSS Statistics 20 license (student's version)	1	2460	2460
			11330.23

Table 10.1. Summary of the material costs.

Personnel costs (unit cost per working day)

The present work is an investigation project conducted by a UPC Biomedical Research engineer and an Industrial engineering degree student. The details indicated in this section concern the software code creation to carry out the algorithms, the familiarization with software and the documentation. It has been considered an estimated salary for a grant holder of approximately 8€/hour (that is the minimum price received by a UPC student during a traineeship). Moreover, the number of working hours that are taken into account are four hours per day, and the dedication includes the working weekdays. The details of the personnel costs are shown in Table 10.2.

Type of expenditure	Number of hours	Unitary price (€/h)	Total amount (€)
Material costs	40	15	600
Personnel costs	850	8	6800
			7400

Table 10.2. Summary of the personnel costs.

Therefore, the total estimated costs are in the Table 10.3.:

Types of costs	Price (€)
Material costs	11330.23
Personnel costs	7400
	18730.23

Table 10.3. Summary of the personnel costs.

A plausible scenario that should be taken into consideration is that there is no possibility to face the license costs (Matlab, Microsoft Office and IBM SPSS). If that was the case, a possible alternative solution could be:

- Complete portability of the system to a Linux-based environment. This would involve the following changes:

  o Recompilation of the software to a Linux environment (that is no problem since there is a Linux compiler adapted to standard C libraries).
  o Translation of the Matlab code into C code: this entails an additional investment in developing new software. This alternative has the problem that the C language does not have all the graphic libraries that are used during results' plotting. For this reason, if a Human-Machine-Interface wants to be designed in order to take advantage all the C languages possibilities, then, a good recommendation would be to use the Java language with the library jfreechart (due to it is an API, namely Application Programing Interface, used in advanced plotting) and the swt APLI (used in Human-Machine-Interface implementation).

Acknowledgements

I express my special gratitude to Professor Pere Caminal, director of the Research Center for Biomedical Engineering (CREB) of the Polytechnic university of Catalonia (UPC), for showing me the interesting world of the Biomedical Engineering.

A special thanks is expressed to the Research Engineer Dra. Montserrat Vallverdú, for being helpful, kind and for her guidance and encouragement to pursue my dreams towards a Biomedical Engineering career. I take with me all her advice and wisdom during the last few years of hard working.

I would like to mention Dr. Pedro Gambús and Erik W. Jensen, for being a professional inspiration and a helping hand during the realization of the thesis.

This work is a result of several projects carried out in industry, research institutes and a university hospital in Barcelona. It has been a rewarding experience to work with all these people, each representing top knowledge in their own specialty.

I wish to thank my parents, Albert and Glòria for their unconditional support. They have encouraged me in the most important and challenging decisions in my life. Although they have possibly made many mistakes, they are the best teachers. Also, I would like to acknowledge the rest of the family my brother Nil, my grandparents (Mercè and Josep), Joan and Esther for making me who I am.

Finally, I would like to acknowledge my dear Berta for her love, patience, and understanding.

Bibliography

References

[1] Prys-Roberts C, "A practical or impossible construct (editorial) ," *Br J Anaesthesia* 59:1341-1345, 1987.

[2] Eger El II, Saidman LJ, Brandstater B, "Minimal alveolar anesthetic concentration: A standard of anesthctic potency," *Anesthesiology* 26:756-763, 1965.

[3] T. W. Bouillon, "Pharmacodynamic interaction between propofol and remifentanil regarding hypnosis, tolerance of laryngoscopy, bispectral index, and electroencephalographic approximate entropy," *Anesthesiology*, vol. 100, 2004, pp.1353-1372.

[4] D. R. Stanski and S. L. Shafer, "Measuring depth of anesthesia," *in Miller's Anesthesia*. 6th ed. vol.1, R. D. Miller, Ed.. Churchill Livingstone, 2004, pp. 1227-1264.

[5] L. Xiaoli, L. Duan, L. Zhenhu, L. Voss, and J. W. Sleigh, "Analysis of depth of anesthesia with Hilbert–Huang spectral entropy," *Clinical Neurophysiology*, vol. 119, 2008, pp. 2465–2475.

[6] R. Ferenets, T. Lipping, A. Anier, V. Jäntti, S. Melto, and S. Hovilehto, "Comparison of entropy and complexity measures for the assessment of depth of sedation," *IEEE Trans. On Biomedical Engineering*, vol. 53, no. 6, June 2006, pp. 1067- 1077.

[7] P. Gifania, H. R. Rabieea, M. H. Hashemib, P. Taslimia, and M. Ghanbari, "Optimal fractal-scaling analysis of human EEG dynamic for depth of anesthesia quantification," *Journal of the Franklin Institute*, vol. 344, 2007, pp. 212–229.

[8] Barnett TP, Johnson LC, Naitoh P, Hicks N, Nute C, "Bispectrum analysis of EEG signal during waking and sleeping," *Science* 1971; 172:401-2.

[9] Veselis RA, Reinsel RA, Wronski M, Marino P, Tong WP, Bedford RF, "EEG and memory effects of low-dose infusions of propofol," Br J *Anesthesiology* 1992; 69:246-54.

[10] Veselis RA, Reinsel R, Sommer S, Carlon G, "Use of neural network analysis to classify electroencephalographic patterns against depth of midazolam sedation in intensive care unit patients," *J.Clin Monit* 1991," 7:259-67.

[11] Kroboth PD, Smith RB, Erb RJ, " Tolerance to alprazolam after intravenous bolus and continuous infusion. Psychomotor and EEG effects," *Clin Pharmacol Ther* 1988; 43:270-7.

ETSEIB

[12] Vernon JM, Lang E, Sebel PS, Manberg P, "Prediction of movement using bispectral electroencephalographic analysis during propofol/alfentanil or isoflurane/alfentanil anesthesia," *Anesth Analg* 1995; 80:780-5.

[13] Rampil IJ, Matteo RS, "Changes in EEG spectral edge frequency correlate with the hemodynamic response to laryngoscopy and intubation," *Anesthesiology* 1987; 67:139-42

[14] Fleischer JE, Milde JH, Moyer TP, Michenfelder JD, "Cerebral effects of high-dose midazolam and subsequent reversal with Ro15-1788 in dogs," *Anesthesiology* 1988; 68:234-42.

[15] Hudson RJ, Stanski DR, Saidman LJ, Meathe E, "A model for studying depth of anesthesia and acute tolerance to thiopental," *Anesthesiology* 1983; 59:301-8.

[16] J. C. Sigl and N. G. Chamoun, "An introduction to bispectral analysis for the EEG," *J. Clin. Monit.*, vol. 10, 1994, pp. 392-404.

[17] H. Viertiö-Oja, V. Maja, M. Särkelä, P. Talja, N. Tenkanen, H. Tolvanen-Laakso, M. Paloheimo, A. Vakkuri, A. Yli-Hankala, and P. Meriläinen, "Description of the Entropy algorithm as applied in the Datex-Ohmeda S/5 Entropy Module", *Acta Anaesthesiol. Scand.*, vol.48, no. 2, 2004, pp. 154–161.

[18] E. W. Jensen, P. Lindholm, and S. Henneberg, "Auto Regressive Modeling with Exogenous Input of auditory evoked potentials to produce an on-line depth of anaesthesia index," *Methods of Information in Medicine*, vol. 35, 1996, pp. 256–260.

[19] H. Litvan, E. W. Jensen, J. Galan, J. Lund, B. E. Rodriguez, S. W. Henneberg, P. Caminal, and J. M. Villar Landeira, "Comparison of conventional averaged and rapid averaged, autoregressive-based extracted auditory evoked potentials for monitoring the hypnotic level during propofol induction," *Anesthesiology*, vol. 97, no. 2, 2002, pp. 351–358.

[20] J. F. Valencia, X. Borrat, and P. L. Gambus, "Validation of a new index, qcon, for assessment of the level of consciousness during sedation," presented at ASA Annual Meeting, Washington, DC, US, October 13-17, 2012, Abstract A640.

[21] T-P. Jung, C. Humphries, T.W. Lee, M.J. McKeown, V. Iragui, S. Makeig, and T.J. Sejnowski, "Removing electroencephalographic artifacts by blind source separation," *Psychophysiology*, 37:163-178, 2000.

[22] D.A. Overton and C. Shagass, " Distribution of eye movement and eye blink potentials over the scalp," *Electroencephalography and Clinical Neurophysiology*, 27:546, 1969.

[23] W.T. Blume, M. Kaibara, and G.B. Young, " Atlas of Adult Electroencephalography," Lippincott Williams and Wilkins, Philadelphia, 2002.

[24] Loeser, J. D.; Treede, R. D. (2008) , " The Kyoto protocol of IASP Basic Pain Terminology".

[25] Portenoy, Russell K.; Brennan, Michael J. (1994) , "Chronic Pain Management".

[26] Kathryn Bayne, "Assessing Pain and Distress: A Veterinary Behaviorist's Perspective. Definition of Pain and Distress and Reporting Requirements for Laboratory Animals (Proceedings of the Workshop Held June 22, 2000)".

[27] Momin, A.; McNaughton, PA. (2009), "Regulation of firing frequency in nociceptive neurons by pro-inflammatory mediators".

[28] Purves, D. (2001), "Nociceptors," In Sunderland, MA.

[29] V. Lalitha and C. Eswaran, (2007) "Automated Detection of Anesthetic Depth Levels Using Chaotic Features with Artificial Neural Networks," *J Med Syst*, 445-452.

[30] Alan T.Hope and Roman Rosipal, "Measuring Depth of Anesthesia using Electroencephalogram Entropy Rate".

[31] Franz Hlwatsch and François Auger, "Time-Frequency Analysis".

[32] R. Bender, B. Schultz, and U. Grouven, (1992) "Classification of EEG signals into general stages of anesthesia in real time using autoregressive models," *Conf Proc of the 16th Annual Conference of the Gesellschaft fur Klassifikatione*, University of Dortmund.

[33] J.C. Sigl and N.G. Chamoun. 1994, "An introduction to bispectral analysis for the electroencephalogram," *Journal of Clinical Monitoring* 10, no. 6, pages 392-404.

[34] T.P. Barnett, L.C. Johnson, P. Naitoh, N. Hicks, and C. Nute. 1971, "Bispec-trum analysis of electroencephalogram signals during waking and sleeping," *Science* 172, no. 3981, pages 401-402.

[35] G. Dumermuth, P.J. Huber, B. Kleiner, and T. Gasser. 1971, "Analysis of in-terrelations between frequency bands of the EEG by means of the bispectrum: a preliminary study," *Electroencephalography and Clinical Neurophysiology* 31, no. 2, pages 137-148.

[36] J. Jeong, "EEG dynamics in patients with Alzheimer's disease," *Clin. Neurophysiology*, 115:1490-1505, 2004.

[37] M.A. Ramsay, T. M. Savege, B. R. Simpson, and R. Goodwin, "Controlled sedation with alphaxalone-alphadolone," *Br. Med. J.*, vol. 2, 1974, pp. 656–659.

[38] U. S. P. Melia, F. Claria, M. Vallverdu, and P. Caminal, "Removal of Peak and Spike Noise in EEG Signals Based on the Analytic Signal Magnitude," *Proc. IEEE- EMBS Conf*, 2010, pp. 3523-3526.

[39] Guzzetti, S., Borroni, E., Garbelli, P.E., Ceriani, E., Della Bella, P., Montano, N., Cogliati, C., Somers, V.K., Malliani, A. and Porta, A., "Symbolic dynamics of heart rate variability. A probe to investigate cardiac autonomic modulation," *Circulation*. v112.465.

[40] D. Cysarz, A. Porta, N. Montano, P.V. Leeuwen, J. Kurths and N. Wessel, "Quantifying heart rate dynamics using different approaches of symbolic dynamics," *Eur. Phys. J Special Topics* 222, pp. 487–500, June 2013.

Complementary bibliography

[41] David S. Moore , "The Basic Practice of Statistics with Cdrom 2nd, " W. H. Freeman & Co. New York, NY, USA$^©$ 1999.

[42] Dale, M. M., Rang, H. P., & Dale, M. M. (2007), "Rang & Dale's pharmacology, " Edinburgh: Churchill Livingstone.